Engineering Structures 237 (2021) 112188

Contents lists available at ScienceDirect

Engineering Structures

journal homepage: www.elsevier.com/locate/engstruct

Spalling of concrete cover induced by reinforcement

Francesco Moccia *, Miguel Fernández Ruiz, Aurelio Muttoni

Ecole Polytechnique Fédérale de Lausanne, School of Architecture, Civil and Environmental Engineering, Lausanne, Switzerland

ARTICLE INFO

Keywords:
Cover spalling
Bond
Radial pressure
Corrosion
Casting position effect
Size effect
Group effect
Concrete tensile strength
Pull-out tests

ABSTRACT

This paper investigates the phenomenon of cover spalling in reinforced concrete induced by bond or by the action of an inner pressure. This research is based on an experimental programme comprising a series of bond tests and a series of tests with inner-pressure on cylindrical openings. The inner-pressure test series (aimed at representing the conditions occurring for instance due to corrosion of reinforcement) was performed with hydraulic inflator devices embedded within concrete openings near to the free concrete surface. By means of detailed surface measurements performed with Digital Image Correlation, the mechanisms triggering spalling failures and the associated resistance are discussed and analysed thoroughly. This series investigates in addition a number of phenomena relevant to spalling failures, such as the influence of the casting position, group and size effects. The observed response, analysed by means of a mechanical analogy, is later used to investigate a series of structural tests performed on pull-out specimens. This analysis highlights the analogies and differences between the two types of tests (subjected to an imposed pressure or to bond stresses). On that basis, a comprehensive approach for treatment of bond-related cases failing by cover spalling is proposed, showing consistent agreement to the experimental evidence.

1. Introduction

Spalling of the concrete cover is a complex phenomenon that influences not only the ultimate limit state of a concrete member, but also its serviceability response and its durability. Spalling failures originate when a transverse force acting near to the concrete surface (originated by the presence of the reinforcement in the investigated cases) equals the tensile resistance of the concrete cover. The actions originating spalling failures can have different sources, as stresses associated to bond between reinforcing bars and surrounding concrete (Fig. 1a) [1–3], the volume expansion due to corrosion of the steel reinforcement (Fig. 1b) [4–8], deviation forces related to detailing with reinforcement bent in parallel to the surface (Fig. 1c) [9–11] or in curved members (Fig. 1d) [12–16], dowel action (Fig. 1e) [17–21] or vapour-pressure under fire conditions [22,23]. The spalling resistance depends in these cases upon a number of factors [3], such as the layout and dimensions of the reinforcing bars, the concrete cover and its strength or the casting position.

In this paper, the phenomenon of spalling in structural concrete is investigated with reference to the action of a radial transverse pressure (as that originated by bond between reinforcement and concrete, Fig. 1a, or associated to volumetric expansion of corroded reinforcement, Fig. 1b). First, an extensive review of the state-of-the-art is presented, followed by a specific testing programme. The experiments were performed both on specimens subjected to inner-pressure acting on cylindrical opening (44 tests) as well as on anchorages (12 pull-out tests). With this programme, a special focus is set on the analysis of the relationship between pull-out failures and the applied transverse pressure, on the influence of the cover thickness and casting position as well as on the size and group effects. This programme was in addition instrumented with Digital Image Correlation, allowing to track in a detailed manner the development of surface cracking and to investigate on the associated load-carrying actions. On the basis of these results, a design approach is proposed based on a simple mechanical model. The consistency of such approach is validated with the test results of this paper as well as with others gathered from the scientific literature.

2. Review of the state-of-the-art

A large number of studies have been performed in the past with reference to spalling failures of concrete. In this section, the most relevant works concerning spalling due to engagement of bond stresses or by application of internal pressures inside concrete will be reviewed. The aim will be to clarify the phenomena triggering spalling failures and to relate them to the experimental programme presented in the next

* Corresponding author.
E-mail addresses: francesco.moccia@epfl.ch (F. Moccia), miguel.fernandezruiz@epfl.ch (M. Fernández Ruiz), aurelio.muttoni@epfl.ch (A. Muttoni).

https://doi.org/10.1016/j.engstruct.2021.112188
Received 13 October 2020; Received in revised form 3 February 2021; Accepted 3 March 2021
Available online 4 April 2021

Nomenclature

Notation

c_x, c_y	cover thickness in x, y direction
c_s	clear spacing
d_g	maximum aggregate size
d_{dg}	average roughness
f_b	bond strength
$f_{c,cyl}$	compressive strength of concrete cylinder
$f_{c,28}$	compressive strength of concrete at 28 days
f_{ct}	tensile strength of concrete
$f_{ct,28}$	tensile strength of concrete at 28 days
f_R	bond index
f_{sp}	radial splitting stress
f_t	reinforcement tensile strength
f_v	vertical force per unit length
f_y	mean value of the yield strength of reinforcement
l_b	anchorage length
n	number of disturbances
m	slope
p	pressure
p_e	external pressure
p_{max}	pressure at peak
$p_\perp$	pressure perpendicular to the cover
$p_{//}$	pressure parallel to the cover
s_c, s_{ct}	coefficients for strength development in time
u_x, u_y, u_z	displacements in x, y, z direction
w_n	crack opening
w_t	crack sliding
W/C	water-to-cement ratio
γ	crack inclination
δ	relative displacement between steel and concrete (slip)
η_{ct}	strength reduction factor to account for concrete brittleness in tension
η_{is}	strength reduction factor to account for casting position effects
θ	inclination of compressive strut to bar axis
λ	coefficient defining the contribution of the splitting components
σ_{agg}	normal stress
σ_{sp}	confining stress
τ_{agg}	shear stress
τ_{avg}	bond stress averaged along anchorage length
ϕ	diameter
ψ	angle defining the crack geometry

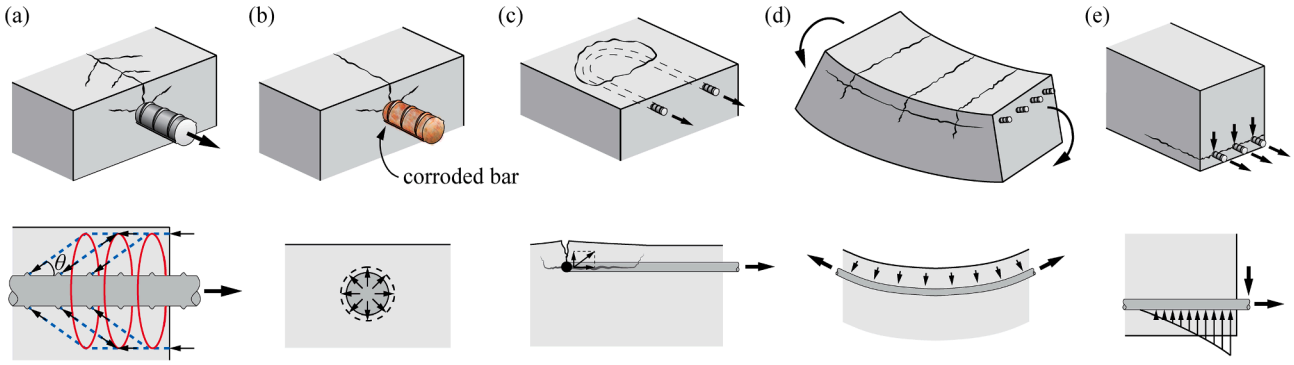

Fig. 1. Potential causes of spalling of the concrete cover related to steel reinforcement: (a) bond-induced spalling; (b) corrosion-induced spalling; (c) spalling related to bent reinforcement; (d) spalling induced by deviation forces on curved members; and (e) spalling induced by dowel action.

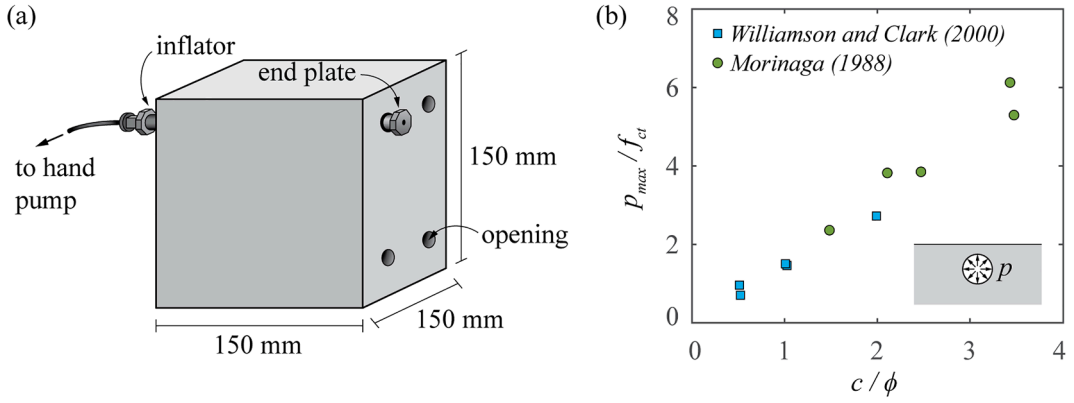

Fig. 2. Uniform internal pressure applied with hydraulic inflator devices: (a) instance of test setup, as described by Williamson and Clark [26]; and (b) normalized maximum pressure applied with inflator devices as function of the cover-to-diameter ratio, adapted from [26].

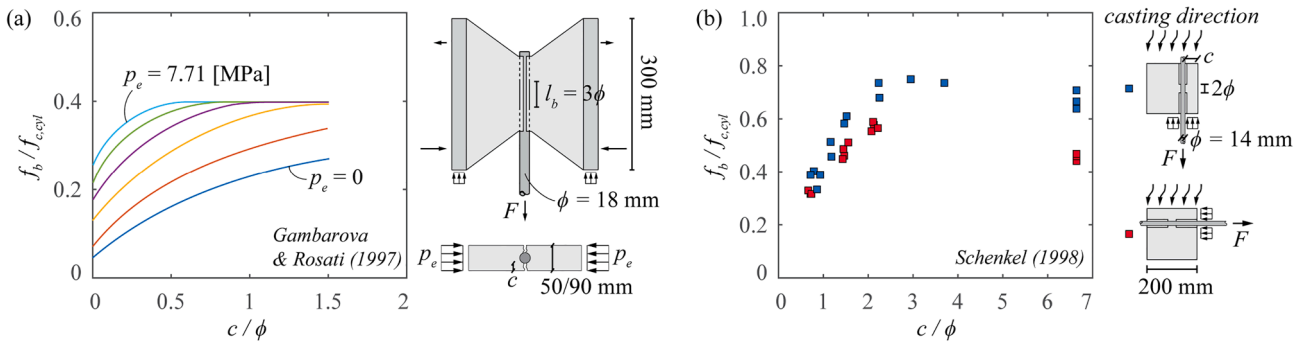

Fig. 3. Influence of cover-to-diameter ratio on the spalling resistance: (a) normalized bond strength as function of the cover-to-diameter ratio and for different values of external pressure (p_e), calculations according to an elastic-cracked-cohesive model, adapted from [38]; and (b) short pull-out tests: normalized bond strength as function of the cover-to-diameter ratio and the casting direction, adapted from [44].

section. Other specific cases related to spalling issues (deviation forces of curved reinforcement or dowel action, Fig. 1c-e) will not be reviewed in detail in this section.

2.1. Influence of internal pressures inside concrete

The application of internal pressures inside openings has been a manner to traditionally investigate the resistance to cover spalling, see Fig. 2. Such approach is in addition suitable to investigate the potential response of corroded reinforcement, where the volumetric expansion of rust acts as an imposed radial displacement generating internal pressures [6–8,24,25].

For instance, Williamson and Clark [26] inserted hydraulic inflator devices within openings located in 150 mm concrete cubes and used a manual pump to pressurize the system (Fig. 2a). The authors varied both the concrete cover and the diameter of the openings (8 mm and 16 mm). A similar study was performed by Morinaga [27] where a uniform pressure was applied within hollow concrete cylinders with variable external diameter (100, 150, 200 mm) and opening diameter (9, 19, 25 mm). Fig. 2b presents the results of the two testing programmes [26,27]. As it can be observed, both programmes have consistently shown an increase on the resistance to internal pressures with increasing values of the concrete cover. In addition, it was noted that for equal thickness of the cover, the maximum pressure reduced with increasing diameter of the openings, indicating the significance of size effect.

In addition, Allan and Cherry [28] simulated local corrosion by injecting oil at the interface between the bar and concrete. It should also be mentioned the work of Noghabai [29], in which pressure was exerted by an inflator placed within concrete cylinders having variable compressive strength and containing in some cases spiral reinforcement.

No specific researches have however been performed so far with such devices on the influence of the casting position, which has been identified as a relevant parameter for the concrete tensile strength and bond [3]. In addition, the outlined experimental programmes were all using pressure-controlled hydraulic pumps (load-controlled tests) and the post-peak behaviour of the cover was thus not recorded in detail. Such response can however be instrumental in cases where potential redistributions of stresses can occur, as in bond failures.

2.2. Spalling induced by bond

Spalling of the concrete cover has been thoroughly investigated in the frame of bond resistance and particularly for the performance of lap joints. Bond stresses are initially developed by the chemical adhesion between steel and hardened concrete. Such adhesion is however relatively low and vanishes at the onset of a relatively small bar slippage. At that moment, the transfer of forces by bond is ensured in ribbed reinforcement by the mechanical engagement between the ribs and the surrounding concrete (Fig. 1a). In assessing the resistance of anchored bars and lap splices, Tepfers [1,30,31] observed that longitudinal cracks appeared in the cover near failure and that these cracks were caused by the tensile stresses related to bond (in accordance to the tension ring shown in Fig. 1a). Longitudinal splitting cracks appear once the stresses reach the concrete tensile strength, which can be governing for the bond strength particularly for bars located near to the concrete surface (where the splitting cracks can lead to spalling of the cover). Following the approach of Tepfers, an analogy can be made between the bond stresses and a radial pressure generated by the rib action (Fig. 1a) according to the following relationship:

$$f_b = f_{sp} \cdot cot\theta \tag{1}$$

where f_b refers to the bond strength, f_{sp} to the internal radial pressure and θ to the angle of the struts with respect to the bar axis (refer to Fig. 1a). Tepfers proposed that an internal angle $\theta = 45°$ could be assumed, although this value has been shown later not to be constant and to depend on the surface roughness (bond index) and considered kinematics [32].

The work of other researchers showed, however, that considering the bond strength is not only dependent on the development of inclined (conical) struts. For instance, Cairns [2,33] observed that the bond strength should be regarded as the sum of two components, one related to the conical struts (associated to the splitting stresses) and a cohesive component depending on the concrete strength. Based on a Mohr-Coulomb failure criterion, the bond resistance was eventually determined as:

$$f_b = f_{sp} \cdot cot\theta + f_{nsp} \tag{2}$$

where f_{nsp} refers to the bond strength related to the cohesive component and thus not related to the internal radial pressure leading to splitting stresses. It is also interesting to note that, following these researches, it was also established the dependence of the bond strength with respect to the orientation of the ribs in relation to the concrete surface where spalling can potentially occur. These researches showed in addition that spalling failures occurred when the concrete cover is smaller than three times the bar diameter, while pull-out failures are governing for higher values of the cover.

Similar results have been obtained recently by Tirassa et al. [32] by using a special test equipment which allows measuring directly the internal radial pressure f_{sp} and with a refined mechanical model which allows calculating the engaged stresses f_{sp} and f_b as a function of the rib geometry and the relative displacement between bar and concrete interface (slip δ and radial displacement w). Both experimental and theoretical results (which are in fine agreement) show that the cohesive component f_{nsp} decreases rapidly with an increase of both displacements (δ and w) and that the angle θ decreases from approximately 50° for small radial displacements to $\theta \approx 15°$ for large radial displacements w. In addition, since the ribs of actual reinforcement bars are not symmetrical

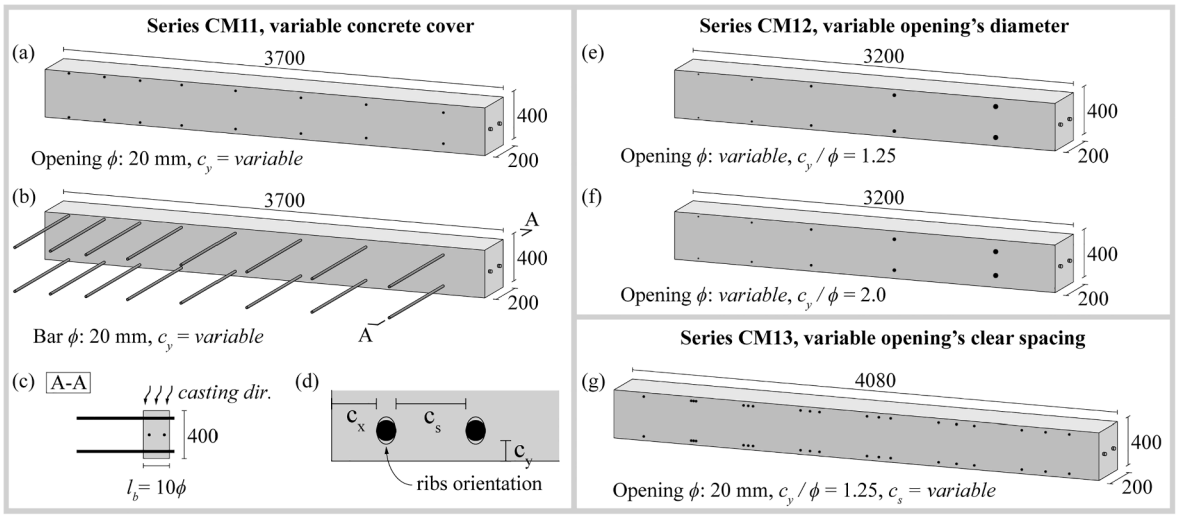

Fig. 4. Geometry and reinforcement of the investigated series (dimensions in [mm], casting direction vertical): (a) specimen with 20 mm openings with variable concrete cover (series CM11); (b) specimen with 20 mm bars with variable concrete cover (series CM11); (c) cross section of prismatic specimen with reinforcing bars of series CM11; (d) definition of clear spacing c_s and concrete cover c_x, c_y in horizontal and vertical direction; (e) specimen with variable opening diameter and ratio $c_y/\phi = 1.25$ (series CM12); (f) specimen with variable opening diameter and ratio $c_y/\phi = 2.0$ (series CM12); and (g) specimen with variable clear spacing between the openings and constant opening diameter and c_y/ϕ ratio (series CM13).

with respect to the bar axis, all parameters can depend significantly on the bar orientation. Further studies on the interaction between bond and splitting stresses were also conducted by Giuriani et al. [34] (refer also to [35,36]) who developed a model taking into account the confining actions of both the transverse reinforcement and concrete cover. These conclusions were also confirmed by Darwin et al. [37] and were followed by a general approach based on limit analysis and considering the influence of concrete cover and transverse pressures formulated by Gambarova et al. [38] (refer also to [39–41]), as shown in Fig. 3a. According to this approach, the application of confining pressures reduces the influence of the concrete cover on the bond strength (as the pressure limits both the crack widths and their extension). In addition, as shown in Fig. 3a, the bond strength exhibits an upper bound related to development of pull-out failures, as well as a shape of the resulting law in agreement to the cohesive component suggested by Cairns [2,33] and later by Malvar [42].

Within the frame of limit analysis, the works of Nielsen and Hoang [43] on spalling failure mechanisms shall also be acknowledged, as well as the considerations of Schenkel [44], accounting for the cracked response of concrete. Schenkel [45] performed in addition a comprehensive experimental programme on pull-out specimens (Fig. 3b), confirming the trends of the previous approaches, notably a potential cohesive component and the transition to pull-out failures.

It is also interesting to note from the tests of Schenkel the significant differences observed depending on the casting direction of pull-out specimens (Fig. 3b). Such effect has also been reported consistently by other researches as [46–50] (an extensive review of this topic can be consulted elsewhere [51]).

3. Experimental programme

An experimental programme was performed at École Polytechnique Fédérale de Lausanne (Switzerland) to investigate on the effects of radial inner pressure on the spalling resistance of concrete. This programme consisted of both inner-pressure tests (where a controlled radial pressure was applied on cylindrical openings within concrete prisms) and structural tests consisting of pull-out tests on embedded reinforcement. The tests were addressed at completing current experimental state-of-the-art and were performed with refined measurements tracking the surface development of cracking. The tests allowed in particular for a detailed analysis of the relationship between failures originated by bond and transverse pressure, the influence of cover and casting conditions as well as the role of size and group effects.

3.1. Description of test series

Three different test series were performed within this programme:

1. Series CM11 (Fig. 4a-d). This series was addressed at the effect of the concrete cover on the spalling resistance under various conditions. In this series, two prismatic specimens were cast with a cross section 0.2 × 0.4 m and a length of 3.7 m. The first specimen (Fig. 4a) presented cylindrical 20-mm openings placed near to the top and bottom surfaces with variable concrete covers (clear cover c varying from 0.25ϕ to 3ϕ). The openings were created by placing plastic tubes fixed to the formwork during concreting (avoiding displacements during concrete consolidation to reproduce the practical case where the reinforcement displacement is prevented by stiff supports) and removing them after hardening of the concrete. These openings were used to apply a radial pressure by means of a hydraulic inflator device later described. The second specimen (Fig. 4b) was nominally identical to the first one, but was cast with two layers of 20-mm steel bars that were tested under pull-out conditions. The bars were fixed to the formwork during casting and had a bond length equal to 10ϕ. All reinforcing bars presented two lugs at opposed sides and the ribs of all bars were aligned perpendicular to the direction of the cover (see Fig. 4d) to ensure uniform conditions amongst them.
2. Series CM12 (Fig. 4e-f). This series was aimed at investigating the influence of the size of the openings on the spalling resistance and was performed on specimens cast with openings (as in Fig. 4a). It consisted of two specimens with identical cross section as series CM11 and a length of 3.2 m. Both specimens presented openings of variable diameter (from 10 mm to 40 mm) arranged near the top and bottom surface. The openings of the first specimen had a constant cover-to-bar diameter ratio (c_y/ϕ) equal to 1.25, while for the second specimen, this ratio was kept constant and equal to 2.0.
3. Series CM13 (Fig. 4g). This series was aimed at the influence of the group effect on the spalling resistance. It consisted of a 4.08 m-long specimens with identical cross section as the previous series. The specimen had 20-mm openings placed in two layers located near to the top and bottom surfaces with constant concrete cover ($c = 1.25\phi$). Isolated top and bottom openings were used as reference

Table 1
Properties and tests results of series CM11, CM12 and CM13 (ϕ: opening or bar diameter; c_y: concrete cover; c_s/c_y: ratio between the clear spacing between multiple openings with respect to their cover; p_{max}: pressure at peak; f_b: bond strength).

Series	ϕ [mm]	c_s/c_y	Top layer				Bottom layer			
			#	c_y/ϕ	p_{max} [MPa]	f_b [MPa]	#	c_y/ϕ	p_{max} [MPa]	f_b [MPa]
CM11	20	–	1	0.25	2.1	–	9	0.25	2.4	–
			2	0.50	2.7		10	0.50	5.2	
			3	0.75	4.1		11	0.75	6.4	
			4	1.0	4.7		12	1.0	7.8	
			5	1.5	6.5		13	1.5	10.4	
			6	2.0	8.4		14	2.0	13.9	
			7	2.5	9.1		15	2.5	17.2	
			8	3.0	–		16	3.0	19.2	
			17	0.25	–	3.1	25	0.25	–	4.7
			18	0.50		3.1	26	0.50		4.9
			19	0.75		3.6	27	0.75		5.0
			20	1.0		5.1	28	1.0		5.6
			21	1.5		–	29	1.5		6.3
			22	2.0		5.6	30	2.0		–
			23	2.5		–	31	2.5		8.1
			24	3.0		7.5	32	3.0		–
CM12	10	–	1	1.25	–	–	6	1.25	11.4	–
	14		2		7.0		7		–	
	20		3		6.2		8		9.5	
	28		4		6.5		9		10.8	
	40		5		6.1		10		8.3	
	10		11	2.0	11.1		16	2.0	–	
	14		12		9.2		17		16.5	
	20		13		9.5		18		15.3	
	28		14		7.9		19		13.1	
	40		15		8.6		20		–	
CM13	20	–	1	1.25	6.9	–	8	1.25	9.6	–
		0	2		1.9		9		2.2	
		1	3		–		10		4.1	
		3	4		5.2		11		9.1	
		4	5		5.9		12		9.7	
		6.5	6		5.7		13		9.8	
		9	7		5.9		14		9.5	

Table 2
Concrete properties and strength ($f_{c,cyl}$ and f_{ct} given at the days of test).

Series	Test type	Cement [kg/m^3]	W/C [–]	Aggregates [kg/m^3]			Retarder [kg/m^3]	Superpl. [kg/m^3]	Age at testing [days]	$f_{c,cyl}$ [MPa]	CoV [%]	f_{ct} [MPa]	CoV [%]
				0/4	4/8	8/16							
CM11	Inflator	342	0.57	893	394	687	1.35	1.70	37–44	39.7	1.6	2.49	3.4
	Pull-out								84–91	42.3	3.9	3.45	4.2
CM12	Inflator								47–54	40.5	2.5	2.78	–
CM13	Inflator								54–62	41.0	2.9	2.90	–

tests, while the rest of the openings were arranged in groups of three with variable clear spacing c_s between them (c_s/c_y ratio from 0 to 9, see Fig. 4g).

Casting of the specimens was consistently performed over the 400-mm height, see Fig. 4. As comparable tests were performed near to the top and bottom surface, the effects of the casting position on the spalling strength [52] could be investigated systematically. In addition to the described openings and bars, all specimens had two 16-mm bars placed longitudinally at mid-height of the cross section to control potential transverse cracks. A summary of the main properties is given in Table 1.

3.2. Materials

The specimens were cast with ordinary ready-mix concrete provided by a local supplier. The cement was CEM II/B-LL 32.5R [53] and the maximum aggregate size was 16 mm. The concrete was poured in two layers of approximately 200 mm, with vibration of the first layer prior to pouring of the second one (casting and vibration conditions according to [54]). During casting, slump and flow tests were performed, ensuring the conditions of [55–57]. A slump of 140 mm was measured (corresponding to class S3) as well as a flow of 480 mm (F3 class). Details on the composition of the concrete are summarized in Table 2.

The concrete compressive strength was assessed by means of 30 concrete cylinders (160-mm diameter with a height of 320 mm) cast with the same batch of the girders. The cylinders were later sealed and cured during 14 days [54], being unmoulded and stored thereafter under the same standard laboratory conditions as for the prismatic specimens (average temperature of 21 °C and average relative humidity of 50%). The cylinders were tested during the complete experimental programme under rapid loading conditions (with failure within approximately 2 min [58]), comprising also tests performed at reference ages (7, 14, 21 and 28 days). In addition, two direct tension tests were carried out on cylinders (identical dimensions as for compression tests) at 28 days and two additional tension tests were performed at the end of the experimental campaign. The compressive and tensile strength at the day of testing for each series was estimated on the basis of the strength development curve of the concrete (using the expressions provided in [59], with coefficients $f_{c,28}$, $f_{ct,28}$, s_c and s_{ct} resulting from best-fit of the test results: $f_c(t) = f_{c,28}\cdot\exp(s_c\cdot(1-(28/t)^{0.5})$ and $f_{ct}(t) = f_{ct,28}\cdot\exp(s_{ct}\cdot(1-$

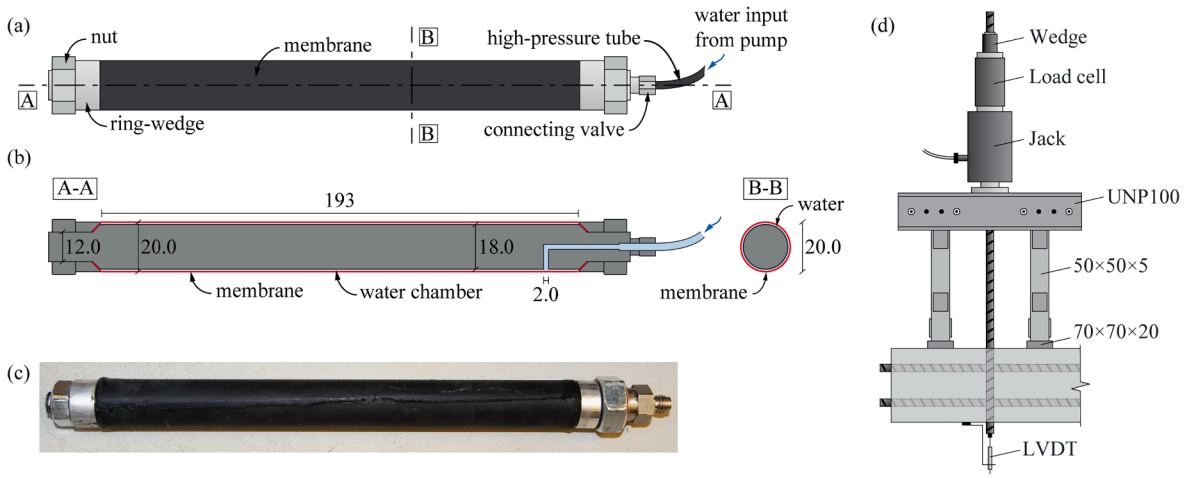

Fig. 5. Testing arrangement (dimensions [mm]): (a) longitudinal view of ϕ20 hydraulic inflator device; (b) longitudinal and cross-sectional view of the hydraulic inflator; (c) photo of an actual hydraulic inflator device; and (d) pull-out setup.

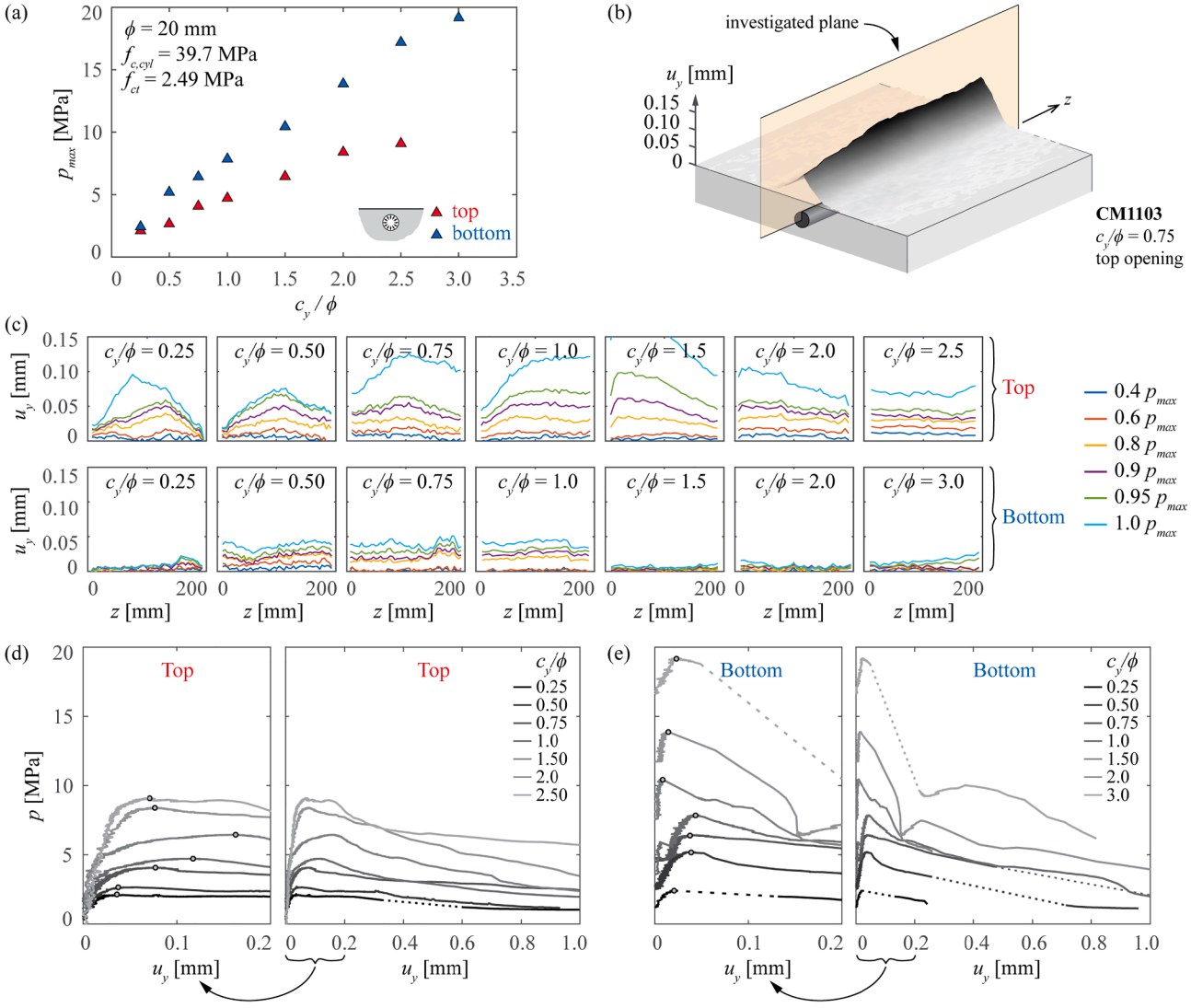

Fig. 6. Main results of test series CM11 with hydraulic inflator devices: (a) maximum pressure reached within the openings as a function of the concrete cover and position (top or bottom layer); (b) instance of the out-of-plane displacement (u_y) measured on the surface; (c) longitudinal distribution of the out-of-plane displacement for several load steps; (d-e) pressure as a function of the maximum out-of-plane displacement recorded on the surface (dotted lines: no recording available; plots to the left correspond to a zoom of the first loading stages with indication of maximum pressure).

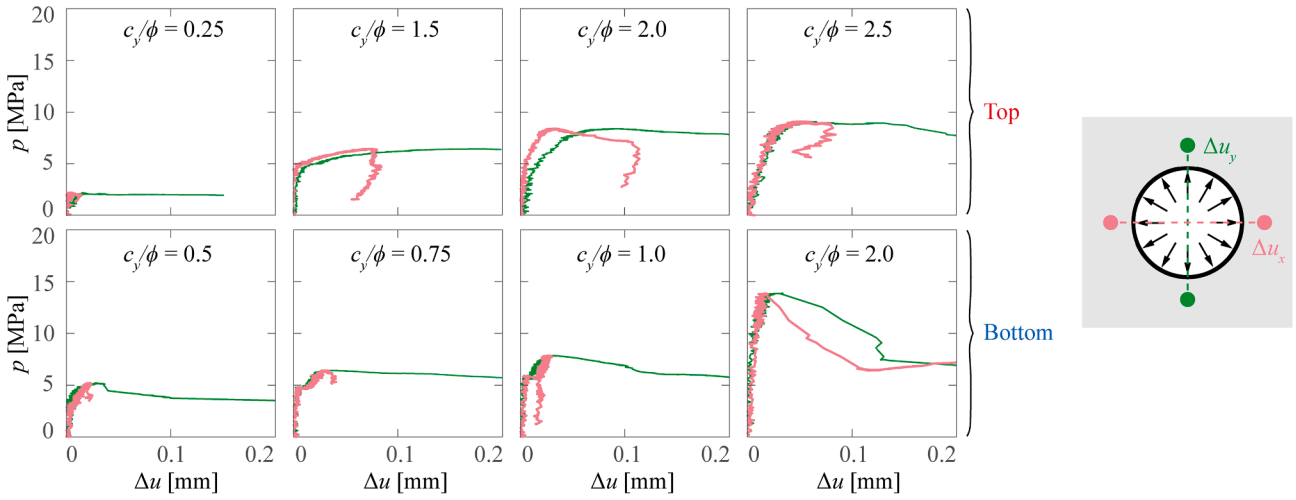

Fig. 7. Vertical and horizontal relative displacements measured with DIC around the openings as a function of the applied pressure for specimens with different concrete cover (green: vertical measurement perpendicular to the free surface, orange: horizontal measurement parallel to the free surface). (For interpretation of the references to colour in this figure legend, the reader is referred to the web version of this article.)

$(28/t)^{0.5}$)). Details for each specimen are provided in Table 2.

The reinforcement steel of the pull-out tests consisted of ϕ20 hot-rolled ribbed bars with a yield strength f_y = 521 MPa (standard deviation equal to 0.7 MPa) and a tensile strength f_t = 620 MPa (standard deviation equal to 1.2 MPa), tested according to [60]. The surface of the bars was laser-scanned to obtain accurate measurements of their rib area and bond index (f_R = 0.072 calculated according to [3]). No tests were performed on the 16-mm bars placed to control transverse cracking (f_{yk} = 500 MPa) as they did not reach characteristic yield strength.

3.3. Instrumentation and setup

3.3.1. Tests with hydraulic inflator devices

Custom-made hydraulic inflator devices of variable diameters (10, 14, 20, 28, 40 mm) were produced to introduce a controlled radial pressure inside of a circular opening (Fig. 5a-c). The devices were inserted into openings located within concrete specimens and were gradually filled with water by means of a pump, providing a uniform radial pressure on the surface of the openings. The inflator has been designed to minimise the volume of introduced water in the device in order to reduce the amount of stored energy during loading (thus allowing for a lower energy release at failure and thus for a stiffer response of the device). Consequently, the hydraulic inflator device was designed with an inner stainless steel tube and an outer membrane, with water only filling their gap (see Fig. 5b).

The external membrane was made of a heat-shrink tube with a nominal thickness of 1 mm that was mechanically processed to obtain the required external diameter. In general, the external diameter was set 0.4 mm smaller than the diameter of the openings to ease their installation. The length of the membrane (193 mm) was slightly shorter than the total length of the openings (200 mm) to avoid development of bumps at their ends. The membrane water-tightness was ensured by two external steel rings tightened by two nuts (Fig. 5a). Tests on water-tightness showed that the device could resist 32 MPa of pressure (maximum capacity of the water pump) without any leakage or degradation. Prior to testing, air has been removed completely from the system.

The pressure in the device was tracked by means of a pressure gauge. Tests performed on air with the device showed that inflating the membrane required approximately 0.3 MPa for a dilatation of the diameter equal to 1 mm. This pressure shows that the stiffness of the membrane is very low and will thus be neglected in the following. Pumping was performed by means of an electronic water pump (GDS ADVDPC 32 MPa [61]) with the following sequence: initial water flow of 8 mm^3/s until a pressure of 0.3 MPa; reduced water flow of 3 mm^3/s between 0.3 and 1 MPa; and finally 1.5 mm^3/s until failure of the concrete cover (tests with a typical duration of 30 min).

3.3.2. Pull-out tests

With respect to the pull-out tests of reinforcement, an adjustable steel frame was used (Fig. 5d). Before testing, the frame was centred to the actual location of the bar and the load was introduced by means of a mechanical hinge (ensuring no transferred bending moment to the bar). The tests were displacement-controlled, with a duration until maximum load of approximately 5 min. The pull-out specimens were instrumented with a linear variable displacement transformer (LVDT) placed at the unloaded-end of the bar (refer to Fig. 5d).

3.3.3. DIC measurements

All tests were monitored with Digital Image Correlation (DIC) using two pairs of high-resolution cameras (Manta G1235B with a resolution of 12.3 Mpix and Manta G419B with 4 Mpix) tracking the surface displacements. The DIC measurements were performed at a frequency of 0.1 Hz at low load levels and were ultimately increased to 2 Hz near failure. The software VIC-3D [62] was used to post-process the data, with a maximum error of approximately 1/25 of a pixel (93 × 93 μm^2 pixel dimension of Manta G1235B, and 116 × 116 μm^2 for Manta G419B).

4. Experimental results

A summary of the measured peak pressure (p_{max}) and bond strength (f_b) are presented in Table 1 for the entire experimental programme. As shown in Table 1, for the tests performed with the hydraulic inflator devices, it was not possible to reach spalling of the cover for six specimens due to the premature failure of the inflator's membrane. These tests will thus not be considered in the following. With respect to the pull-out tests, four bars could not be tested due to the presence of a pre-existing crack originated by a test previously performed on the opposite layer.

4.1. Inner-pressure tests with the hydraulic inflator device

4.1.1. Influence of cover

Series CM11 aimed at investigating the effect of concrete cover and casting position on the spalling resistance. Fig. 6 shows the maximum

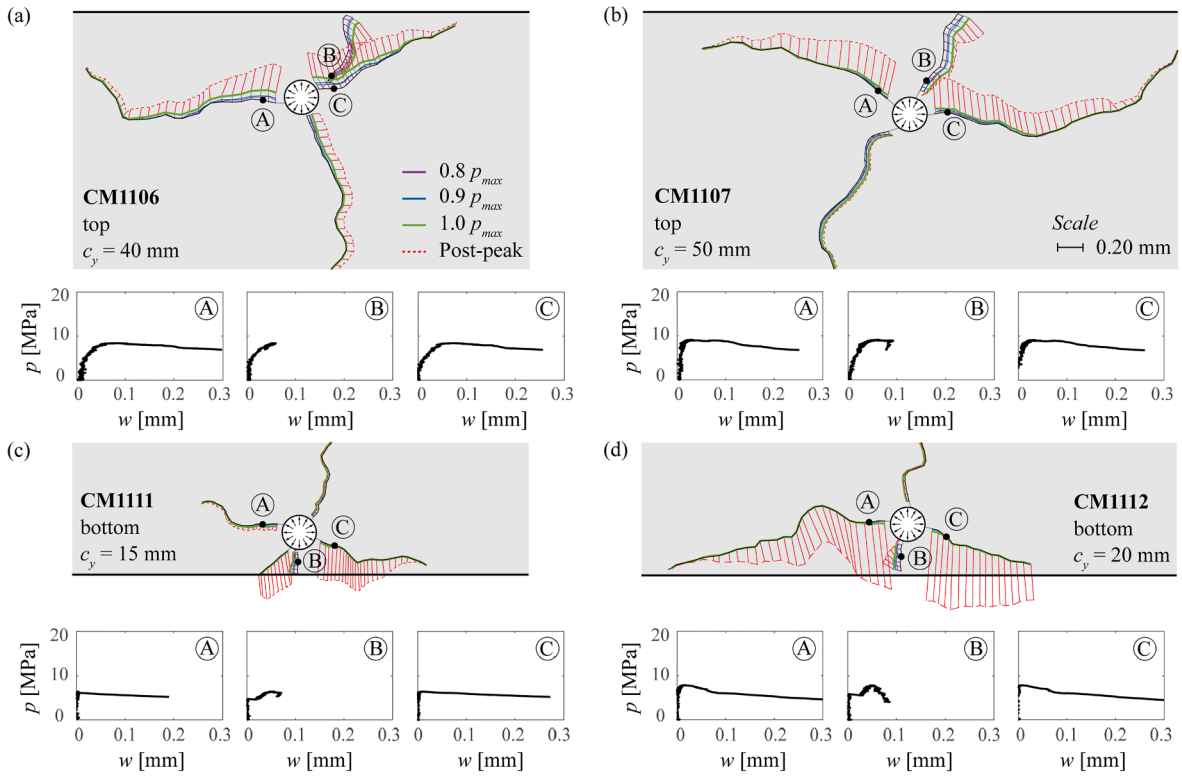

Fig. 8. Crack development and relative crack displacements at selected load steps and crack opening as a function of the applied pressure at selected crack locations (A, B, C): (a) specimen CM1106; (b) specimen CM1107; (c) specimen CM1111; and (d) specimen CM1112.

pressure recorded for this series providing also a detailed overview of the out-of-plane displacements measured with DIC on the top and bottom surfaces.

All tests failed by spalling of the concrete cover. As shown in Fig. 6a, the maximum recorded pressure increases almost linearly with increasing concrete cover and was consistently higher for the bottom position than for the top one. This latter fact indicates that the casting position plays a major role in the spalling resistance of the cover. Such effect can be explained by the reduced concrete tensile strength near to the top surface due to bleeding (in particular in the vertical direction, refer to [63]) as well as by the presence of pre-existing cracks and voids around the openings related to the plastic settlement of fresh concrete [46,52]. More details on this aspect will be discussed later. Also, the trends observed in Fig. 6a are in agreement with those obtained by other authors with similar testing devices [26,27], as shown in Fig. 2b.

Fig. 6b shows the out-of-plane displacements of the free surface for an illustrative test. From such measurements, the profile of out-of-plane displacements along the inflator axis can be determined as depicted in Fig. 6c. This figure shows that the out-of-plane displacements for tests near to the top surface are significantly higher than the corresponding of the bottom layer. In general, out-of-plane maximum displacements of about 0.05–0.15 mm were recorded at peak load on the top surface, while these values were generally smaller than 0.05 mm on the bottom surface.

The recorded pressure as a function of the maximum out-of-plane displacement is also plotted in Fig. 6d-e for the top and bottom surfaces and different cover-to-diameter ratios. As depicted in Fig. 6d, the tests on the top openings showed a relatively tough post-peak behaviour, particularly in case of low concrete covers. On the other hand, the tests on the openings of the bottom layer presented a significantly brittle post-peak behaviour, with a large decrease of the residual capacity for increasing concrete covers (Fig. 6e). In some cases, the increase of out-of-plane displacements was sudden and, despite the high frequency of measurements, it was not possible to follow the entire post-peak response (indicated with dotted lines in Fig. 6d-e). Interestingly, the residual capacity of the bottom openings seems to stabilize to values similar to the ones observed in the post-peak response of the top openings (as both presented comparable cracking patterns and kinematics in the post-peak phase).

A closer look at the evolution of the horizontal and vertical displacements at the sides of the openings (instrumented with DIC) can be seen in Fig. 7 for some selected specimens. According to this Figure, the relative horizontal displacement near top openings appears to have a stiffer response compared to the vertical one (perpendicular to the free surface). The softer response in the vertical direction could be explained by the gradual opening with increasing inner pressure of pre-existing plastic settlement cracks. On the contrary, for bottom openings (in which casting position effects are not relevant), the relative displacement in the vertical and horizontal direction are virtually identical. It can also be noted that the out-of-plane displacement measured on the surface (refer to Fig. 6d-e) corresponds to the relative vertical displacement u_y measured at the side of the elements (Fig. 7).

The DIC measurements performed at the sides of the elements allowed in addition for detailed analyses on the crack patterns and their evolution. Fig. 8 shows for some selected locations the measured crack opening (w) as a function of the applied pressure. The response observed is very different for top and bottom openings. Two representative cases of the top layer are shown in Fig. 8a-b. For these specimens, the cracks developed gradually, with larger crack widths near the circular openings. The spalling failure mechanism was characterized by the development of two concrete wedges formed at each side of the bar. With respect to the cracks, an opening was recorded even at low pressures (refer to graphs of points A, B, C). This implies that the cracks already existed prior to testing, which can be attributed to the plastic settlement of fresh concrete [52,64]. The phenomenon of plastic settlement has thus a direct impact on the position and shape of the cracks and, eventually, also on the failure mechanism of the investigated specimens.

With respect to the openings of the bottom layer (Fig. 8c-d), the crack

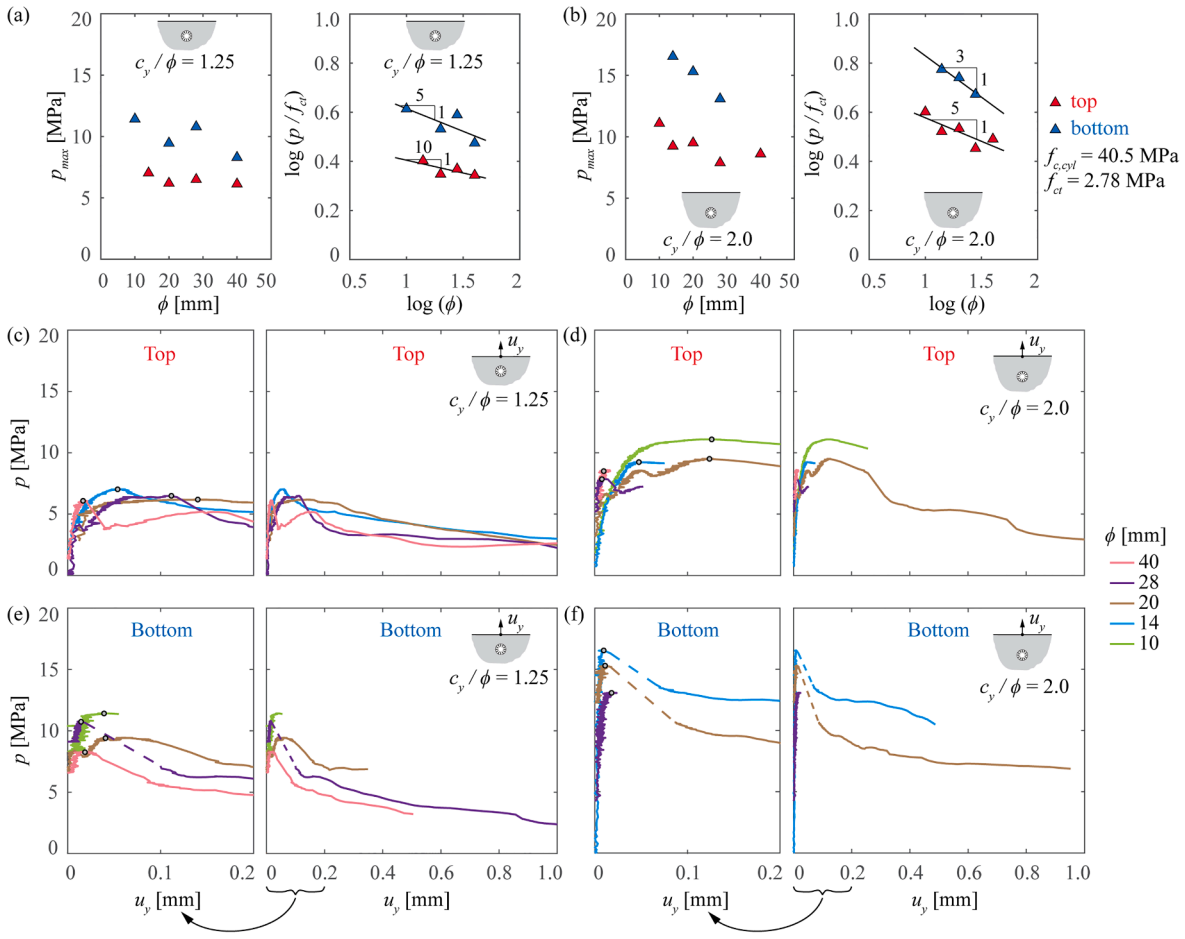

Fig. 9. Main results of test series CM12: (a-b) maximum pressure as a function of their diameter and position (top or bottom layer) for $c_y/\phi = 1.25$ and $c_y/\phi = 2.0$ as well as representation in double-log scale; (c-f) applied pressure as a function of the maximum out-of-plane displacement recorded on the surface (top or bottom layer) for a cover-to-diameter ratio of 1.25 and 2.0.

development was significantly different. In fact, prior to failure, only the vertical crack towards the surface developed, a phenomenon that occurred at approximately 70–80% of the maximum pressure (refer to graphs of point B in Fig. 8c-d). All other cracks developed suddenly at the peak value of the pressure. The crack propagation was thus unstable, showing a very brittle behaviour. It should also be pointed out that, for both top and bottom openings, the inclination and shape of the cracks was different for each test, implying a variety of potential failure mechanisms.

4.1.2. *Influence of size of the opening (size effect)*

Series CM12 was aimed at investigating the influence of the size of the openings on the spalling resistance. Fig. 9a-b depicts the peak value of the pressure as a function of the diameter and position of the openings as well as their representation in double-log scale. The out-of-plane displacements (based on DIC measurements) are also plotted in Fig. 9c-f as a function of the applied radial pressure.

As shown in Fig. 9a-b, the maximum pressure recorded appears to decrease with increasing diameter of the openings. This result is consistent both for the top and bottom layers as well as for cover-to-diameter ratios of 1.25 and 2.0. In addition, it can be noted that the strength decrease with increasing size is more pronounced for larger cover dimensions (Fig. 9b). These observations give evidence of the significance of size effect when dealing with spalling failures. The measured slopes of the size effect in double-log scale for the specimens with small cover ($c/\phi = 1.25$) leads to an approximate slope of −1:5 for bottom openings and to a slope of −1:10 for top openings. This is in accordance with a significantly more brittle response for bottom openings. These slopes are in any case clearly milder than the one corresponding to a behaviour governed by linear-elastic fracture mechanics (−1:2) according to the size-effect law for bond [65]. They indicate thus that nonlinear fracture mechanics is governing for the response in the range of parameters investigated and that some level of redistribution of internal stresses is potentially possible (as for shear-related failures [66,67]). Insufficient experimental data is however available for a complete analysis of the associated size-effect law [65]. With respect to the tests with larger cover ($c/\phi = 2.0$), the measured slopes are higher, −1:3 for bottom openings and −1:5 for top openings, corresponding to a more brittle response (this is also consistent with the more brittle behaviour shown in Fig. 6d-e). As for the low concrete cover specimens, the response of openings located at the bottom is observed again to be more brittle (associated to higher slopes of the size effect in double-log scale).

In a similar manner as for series CM11, the openings located near to the top surface exhibited in all cases smaller peak pressures compared to the openings of the bottom layer. This observation shows again the significance of the casting position effects on the spalling resistance.

Fig. 9c-f presents the load - out-of-plane displacement relationships at the location where the peak value of such displacement was reached. Here again, the tests on the top openings showed a higher out-of-plane displacement at peak pressure and a more ductile behaviour compared to the openings of the bottom layer. However, it seems that larger opening diameters (for instance $\phi = 40$ mm) were associated in almost all cases to lower out-of-plane displacements at failure and to a more

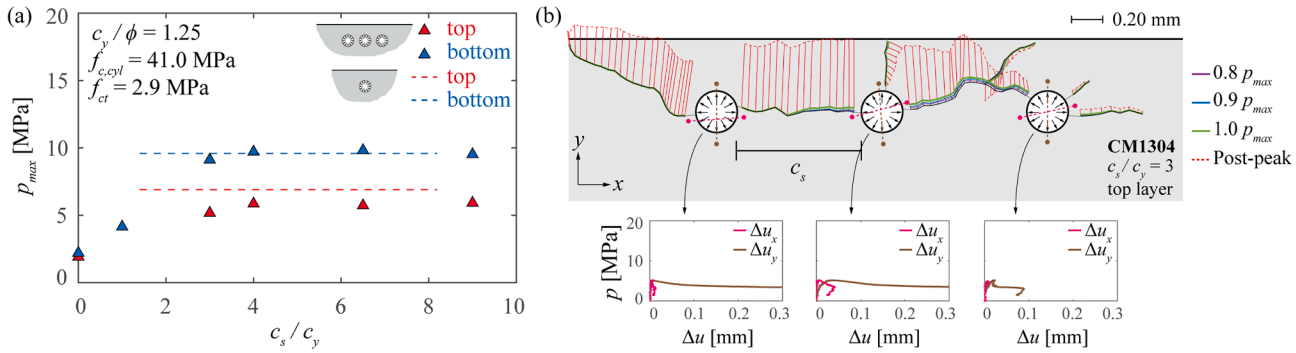

Fig. 10. Main results of test series CM13: (a) maximum pressure as a function of their clear spacing and opening position (top or bottom layer); and (b) specimen CM1304: crack development and relative crack displacements at selected load steps and vertical (Δu_y) and horizontal (Δu_x) relative displacement at each opening.

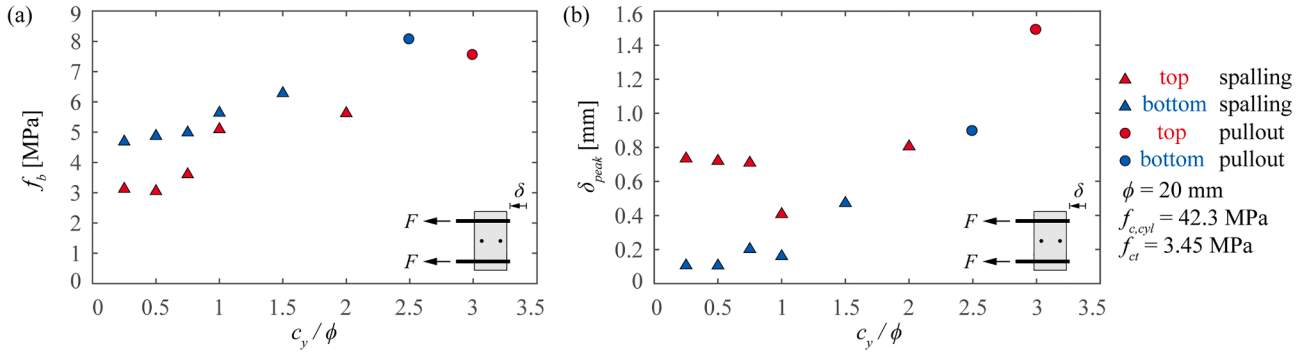

Fig. 11. Main results of the pull-out tests of series CM11: (a) bond strength averaged over the anchorage length as a function of the concrete cover and bar position (top or bottom layer); (b) slip measured at the peak bond strength as a function of the concrete cover and bar position.

brittle post-peak response for both the top and bottom position. With this respect, it has to be observed that the enhanced brittleness could however be also partly attributed to the energy stored in the larger volume of water stored in the inflator device.

4.1.3. *Influence of disturbance spacing (group effect)*

Series CM13 was addressed at investigating the influence of the group effect on the spalling resistance of the cover. Fig. 10a displays the maximum pressure recorded for different values of the clear spacing c_s when compared to a reference (isolated) opening (shown with dashed lines). A representative cracking pattern with the associated displacements is also shown in Fig. 10b.

As depicted in Fig. 10a, for groups of widely spaced openings ($c_s/c_y > 3$), the peak strength reaches similar values as the one of the

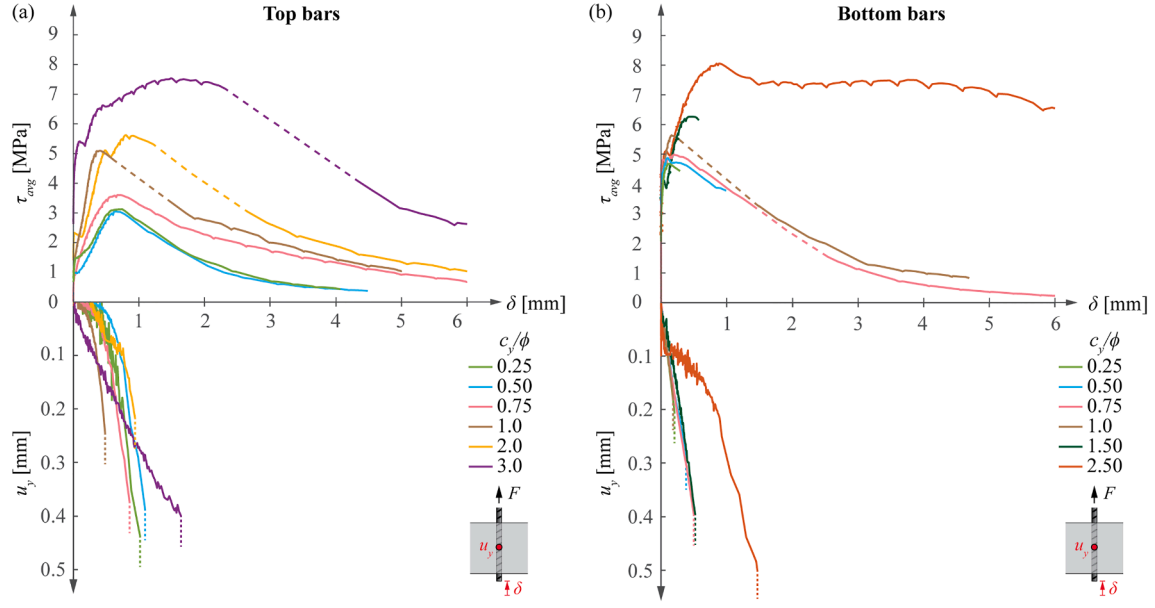

Fig. 12. Bond response and out-of-plane displacement as function of the slip at the unloaded end of the bars (dotted lines: no recording available): (a) top layer; (b) bottom layer.

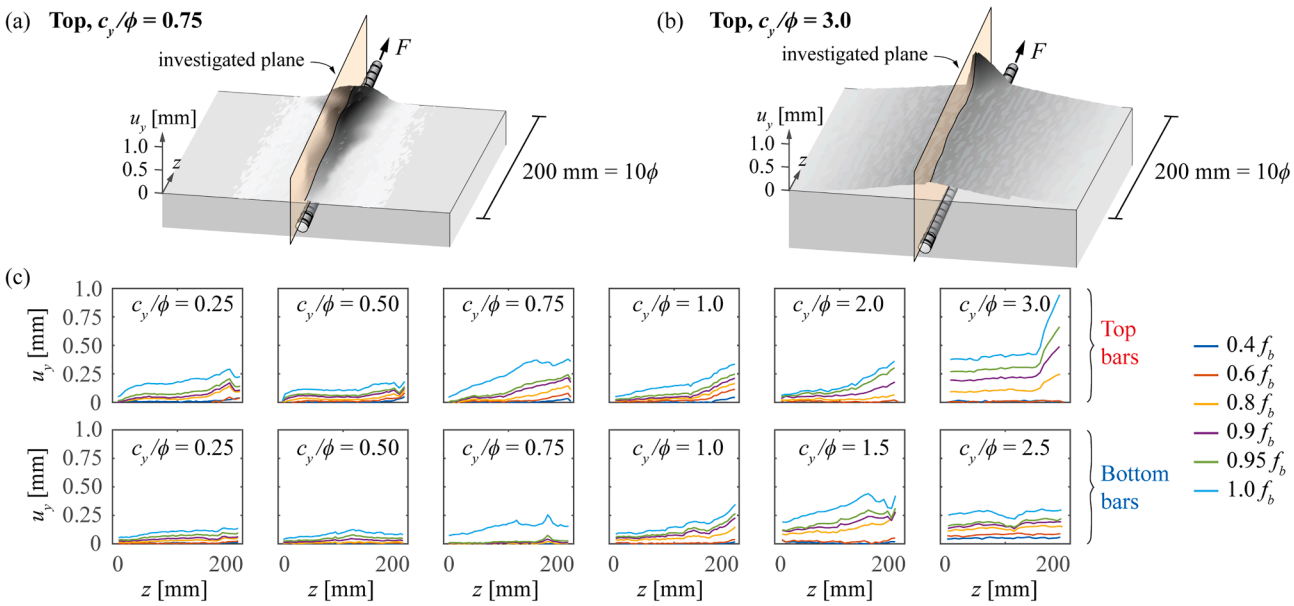

Fig. 13. Out-of-plane displacement (u_y) at failure measured on the surface: (a) specimen CM1119 at peak load; (b) specimen CM1124 at peak load; and (c) longitudinal distribution of the out-of-plane displacement for several load steps and for all pull-out tests.

references with single openings both for top and bottom casting positions (represented with horizontal dashed lines in the Figure). For lower values of the opening spacing ($c_s/c_y < 3$), the resistance is however reduced. This result clearly indicates that the group effect has an influence on the spalling resistance of the cover.

With respect to the detailed cracking pattern shown in Fig. 10b for a specimen influenced by the group interaction (specimen CM1304 with $c_s/c_y = 3$), the crack development differs significantly from that of isolated openings (see for instance Fig. 8). The failure surface develops with a horizontal crack between the different openings and two inclined cracks at the sides plus a quasi-vertical crack (Fig. 10b). As for isolated disturbances, for group of bars, a clear difference is also observed in terms of strength for top and bottom openings, with lower spalling resistances associated to the top position.

4.2. Pull-out tests

With respect to the pull-out tests with embedded length 10ϕ, Fig. 11 depicts the bond strength f_b averaged over the anchorage length and the corresponding slip at peak load δ_{peak} (measured at the unloaded end of the bars) as a function of the cover-to-diameter ratio. The location of the bars with respect to the casting direction (top or bottom layer) as well as the observed failure mode (spalling or pull-out) are also indicated with different colours and symbols.

As shown in Fig. 11a, the bond strength increases for increasing cover of the bars. Such increase seems to follow an almost linear trend, both for the top and bottom reinforcing bars. It can be noted that, even for low values of the concrete cover, a significant bond strength is observed, in accordance to the observations of Cairns and Jones [2]. Spalling failures occurred for cover-to-diameter ratios lower than approximately 1.5–2.0. For higher values, pull-out failures were observed (as also reported by Schenkel [44,45] on short pull-out specimens, refer to Fig. 3b).

With respect to the influence of casting conditions, top bars were observed to provide lower bond strength than the corresponding bottom bars, indicating poorer bond conditions. This response can be attributed to the phenomena of bleeding and plastic settlement [52]. The latter (plastic settlement) is responsible for creating continuous voids under the reinforcement [46,52] as well as inclined cracks reaching the surface [68]. The former (bleeding) influences mostly the tensile resistance of concrete in the top region and can also create large pores under bars or aggregates [63].

With respect to the slip measured at peak load (Fig. 11b), it can be noted that it tends to increase for increasing values of the concrete cover. The phenomenon is however somewhat scattered. Also, the top layer of reinforcement presents larger slips at peak compared to the corresponding bottom layer. This observation can be related to the presence of voids under the bars originated by plastic settlement that requires some slip of the bar to engage the ribs, as discussed more in detail in the following.

Fig. 12 relates the average bond stress, the slip recorded at the unloaded end of the bars and the out-of-plane displacement of the surface (measured with the DIC at the centre of the bond length). Both results for the top layer (Fig. 12a) and bottom layer (Fig. 12b) are

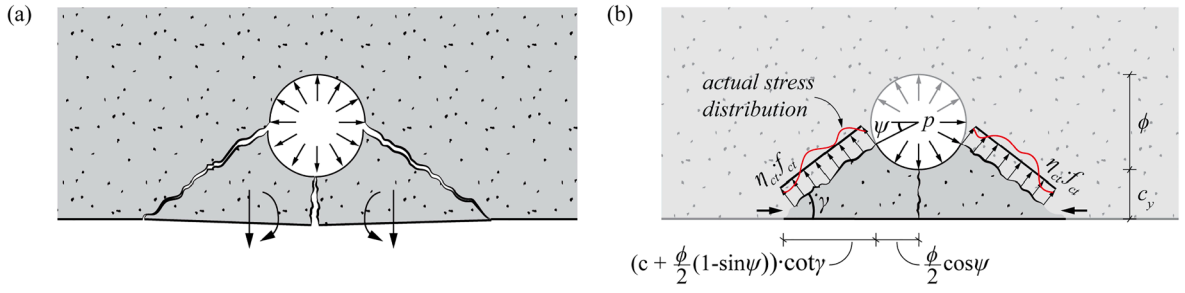

Fig. 14. Idealized model for radial pressure: (a) idealized cover spalling mechanism; and (b) assumed stress distribution along the cracks.

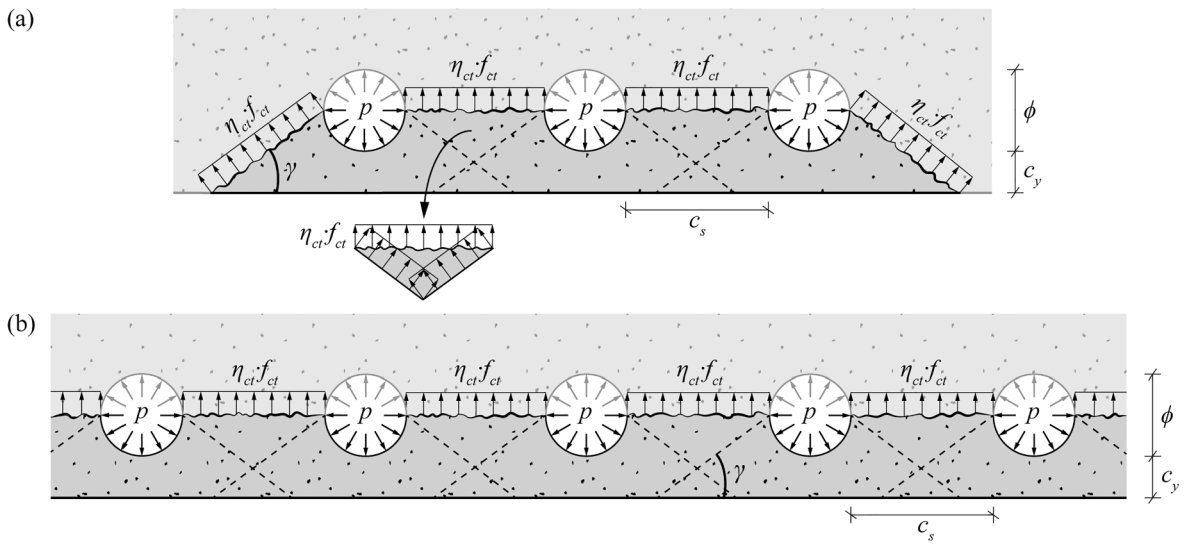

Fig. 15. Spalling failure mechanism in case of multiple openings closely spaced: (a) case with three openings; and (b) case with large number of openings.

presented. It should be noted that it was not possible to record the complete post-peak behaviour at the surface (measured with DIC) due to the significant spalling of the cover once the peak bond strength is reached. On the contrary, the LVDT (placed at the unloaded end of the bar) recorded the slip for the entire post-peak response of most of the bars (refer to Fig. 12).

As shown in Fig. 12a, bars placed in the top layer start to slip at low values of the applied load. This occurs in addition for an almost negligible out-of-plane displacement (particularly for low values of concrete cover), implying that early slip of the bar can occur without developing significant transverse pressures. Such observation can be justified, as previously discussed, by the presence of voids originated by plastic settlement and located under the bars (reducing the contact area between the bar and the surrounding concrete and requiring some level of slip to centre the bar and to engage mechanical contacts [69]). With respect to the bottom reinforcement (Fig. 12b), the voids associated to plastic settlement are negligible and the response is much stiffer, with low slip at early loading stages. In addition, small slips of these bars are accompanied by an out-of-plane displacement on the surface, indicating an almost perfect engagement between the bar and the surrounding concrete from the beginning.

With respect to the post-peak response, the bottom bars showed a relatively brittle response, Fig. 12b, with a sudden drop of resistance once the maximum load was reached. Also, it can be noted that the tests characterized by pull-out failures ($c_y/\phi \geq 3.0$ in the top layer, $c_y/\phi \geq 2.5$ in the bottom layer) exhibit a less brittle behaviour and a larger residual strength compared to test failing by spalling of the concrete cover.

The measured out-of-plane displacements are presented in Fig. 13. The observed profiles are relatively different to those of inner-pressure tests, with maximum values concentrated at the loaded end of the bar,

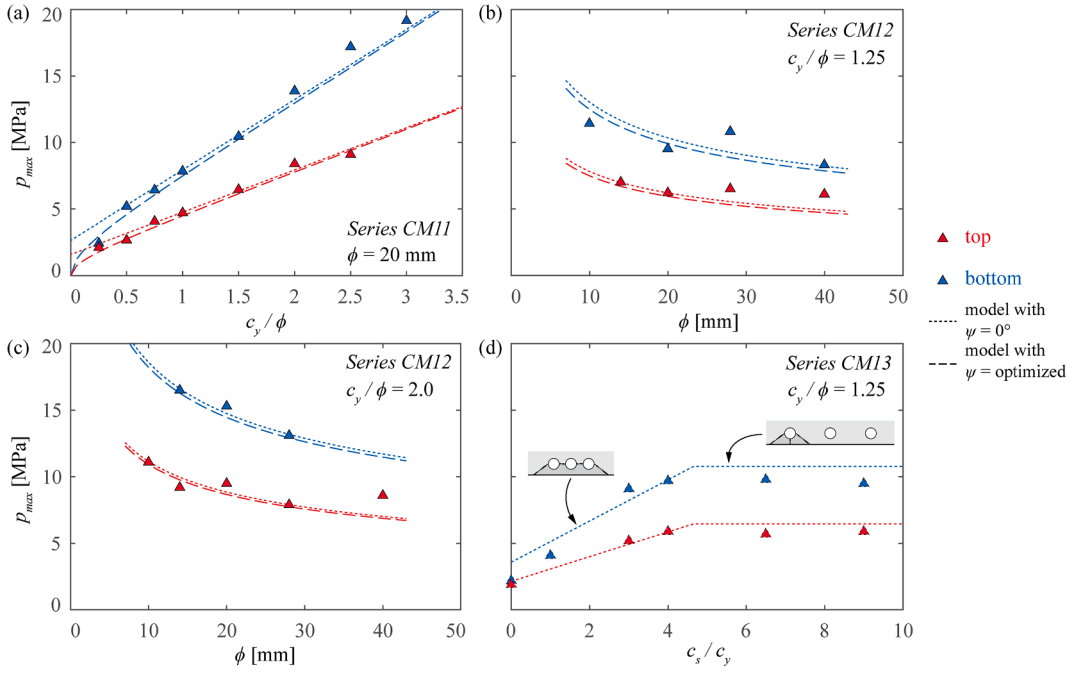

Fig. 16. Main results of the proposed models (refer to Eqs. (10), (14), (17)) for the entire results of the experimental programme (triangle markers): (a) model for top and bottom openings with variable concrete cover (series CM11); (b) model for top and bottom openings with variable diameter (series CM12, $c/\phi = 1.25$); (c) model for top and bottom openings with variable diameter (series CM12, $c/\phi = 2.0$); and (d) model for top and bottom openings with variable spacing (series CM13).

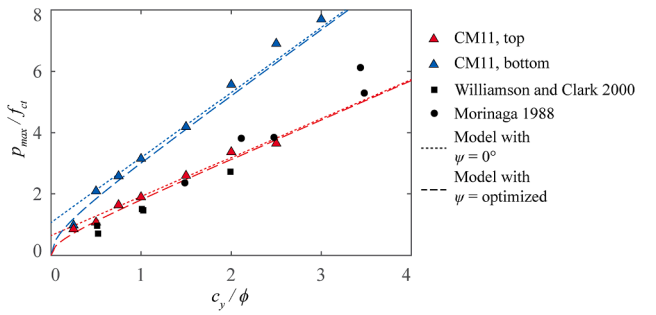

Fig. 17. Comparison of test series CM11 and proposed models with available tests performed with hydraulic inflator devices taken from the literature [26,27].

which can be explained by the higher slips in this region. Fig. 13c shows the distribution of the out-of-plane displacements measured on the surface along the reinforcing bars for selected load steps. The overall out-of-plane displacements seem to increase with increasing concrete cover, both for top and bottom bars. Just before failure, near to the loaded end, large values of the out-of-plane displacement were recorded (u_y above 0.2 mm) indicating that concrete in tension was in its softening regime and that stress redistributions potentially occurred. In addition, some discontinuities can be observed near to the loaded ends (probably related to the development of conical cracks around the bar and reaching the surface, as observed by Goto [70]). Differently to the tests with the hydraulic inflator device, the out-of-plane displacements were similar for top and bottom bars.

5. Design approach for spalling failures due to the application of an internal pressure

On the basis of the previous considerations, a simplified approach can be proposed to assess the spalling strength of bars located near the concrete cover, which is a relevant design issue since similar radial pressures occur in case of bond or for corroded reinforcement. This approach is consistent with previous simplified models [16,43,44], assuming a given geometry for the crack surface and an average strength of the concrete cover in tension.

5.1. Geometrical parameters

Based on the observations of the crack development and kinematics, the spalling failure mechanism is assumed to be characterized by two concrete wedges developing a translation movement and a rotation due to the pressure applied, refer to Fig. 14a.

In this approach, it is assumed that cracks develop from a point located at an angle ψ with respect to the mid-height of the openings and have a linear shape characterized by an inclination γ. As previously shown in Fig. 8, the angle at which these cracks develop is highly variable, both for top and bottom openings. As a simplification of all these cases, the γ angle is set to a constant value assumed such that $\sin\gamma = 0.60$ ($\gamma \approx 37°$).

5.2. Stress distribution and equilibrium of forces

The potentially variable distribution of the tensile stresses along a crack (Fig. 14b) is simplified in the following by assuming an average value of the tensile stress equal to $\sigma_t = \eta_{ct} \cdot f_{ct}$, where η_{ct} accounts for the concrete brittleness in tension and is taken equal to 0.8 (expression considered valid for concrete strengths up to 50 MPa according to [16]). In the following calculations, the mean tensile strength measured in the experimental programme is considered for the definition of f_{ct} (values outlined in Table 2). As shown in Fig. 14b, the vertical component of the concrete tensile stresses is given by:

$$\eta_{ct} \cdot f_{ct} \cdot cos\gamma \tag{3}$$

and the length over which it develops corresponds to:

$$\left(c_y + \phi/2 \cdot (1 - sin\psi)\right) \Big/ sin\gamma \tag{4}$$

The equilibrium condition of the forces acting in the vertical direction leads to:

$$p \cdot \frac{\phi}{2} \cdot cos\psi = \frac{\eta_{ct} \cdot f_{ct}}{tan\gamma} \cdot \left(c_y + \frac{\phi}{2} \cdot (1 - sin\psi)\right) \tag{5}$$

so that:

$$p = \frac{\eta_{ct} \cdot f_{ct}}{tan\gamma} \cdot \frac{2c_y/\phi + (1 - sin\psi)}{cos\psi} \tag{6}$$

According to limit analysis, the governing failure mechanism can be obtained by minimizing:

$$F(\psi) = \frac{2c_y/\phi + (1 - sin\psi)}{cos\psi} \tag{7}$$

so that:

$$sin\psi = \frac{1}{1 + \frac{2c_y}{\phi}} \tag{8}$$

which allows determining the load carrying capacity as:

$$p = \frac{\eta_{ct} \cdot f_{ct}}{tan\gamma} \cdot 2\sqrt{\frac{c_y}{\phi} + \left(\frac{c_y}{\phi}\right)^2} \tag{9}$$

It can be noted that when c_y/ϕ is large, the optimum value is obtained with $\psi \approx 0°$, which corresponds to:

$$p = \frac{\eta_{ct} \cdot f_{ct}}{tan\gamma} \cdot \left(1 + \frac{2c_y}{\phi}\right) \tag{10}$$

Such response is relevant when concrete covers are large, but could also be governing in case pre-existing cracks are present (for instance due to plastic settlement near top bars, refer to Section 4.1 and Fig. 8a-b) and govern the shape of the failure surface. In the following, the formulation of Eq. (9), in which the angle ψ is optimized, is further developed, but considerations will also be performed on the case of $\psi = 0°$.

5.3. Consideration of size effect

The experimental programme has confirmed that peak pressures decrease with increasing size of the openings (refer to Fig. 9), giving evidence of the significance of size effect for spalling failures. This effect is related to the tensile strength of the cover, but also to the opening of the cracks in cases of stable crack opening [66,67] (where larger sizes are associated to larger crack openings and thus to a lower residual tensile strength of concrete). On this basis, Eq. (9) is corrected to account for this effect, adopting the same parameter as for shear-related cases according to prEN 1992-1-1:2018 [71]:

$$p = \frac{\eta_{ct} \cdot f_{ct}}{tan\gamma} \cdot 2\sqrt{\frac{c_y}{\phi} + \left(\frac{c_y}{\phi}\right)^2} \cdot \left(\frac{d_{dg}}{d_{dg0}} \cdot \frac{\phi_0}{\phi}\right)^{1/m} \tag{11}$$

where $d_{dg0} = 32$ mm and $\phi_0 = 20$ mm (reference sizes). It can be noted that the size effect factor accounts for the maximum aggregate size and the bar diameter [71]. This dependence is a simplified approach, as other potentially influencing parameters (for instance the concrete cover) are not explicitly considered. By simplifying the reference sizes, the previous equation becomes:

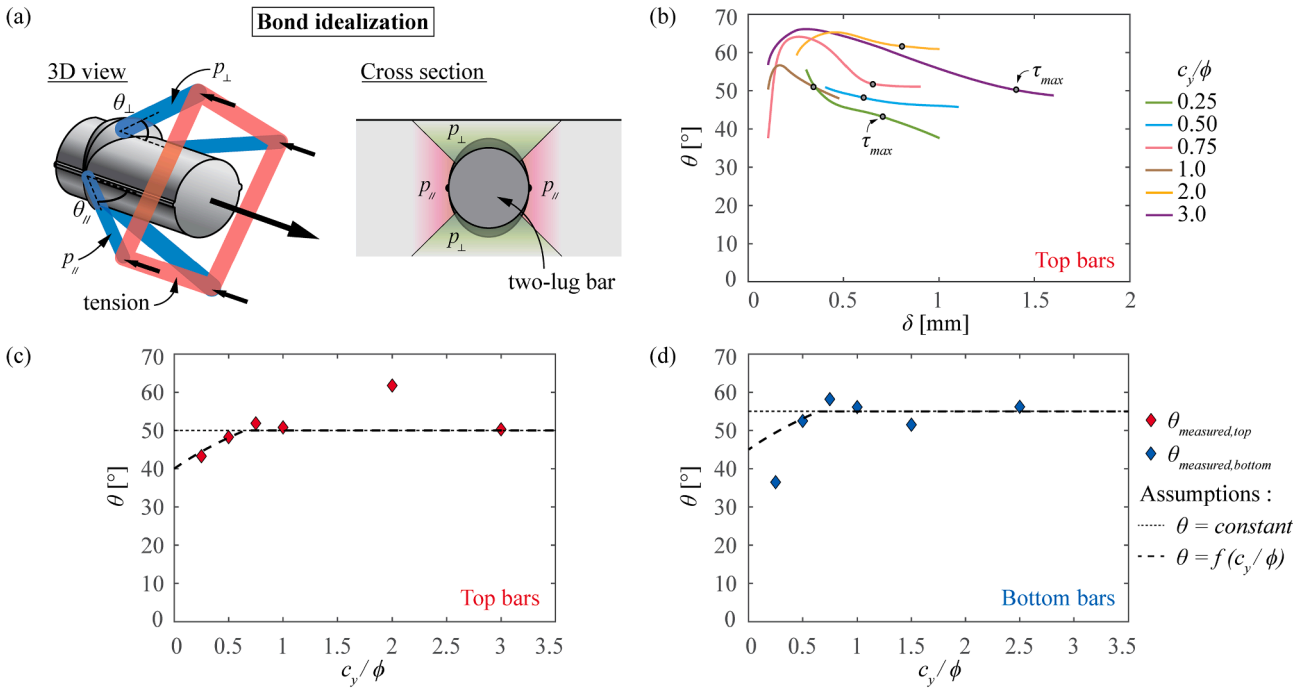

Fig. 18. (a) Idealization of bond strength by means of splitting components $p_{\perp}$ and $p_{//}$; (b) measured average angle of the struts θ as function of the slip δ; (c) measured angle θ at peak bond strength for the top bars of series CM11 and comparison to assumed values of θ; and (d) measured angle θ at peak bond strength for the bottom bars of series CM11 and comparison to assumed values of θ.

$$p = \frac{\eta_{ct} \cdot f_{ct}}{tan\gamma} \cdot 2\sqrt{\frac{c_y}{\phi} + \left(\frac{c_y}{\phi}\right)^2} \cdot \left(\frac{d_{dg}}{1.6\phi}\right)^{1/m} \tag{12}$$

where the d_{dg} parameter is an average roughness whose value can be calculated as [72]:

$$d_{dg} = \min(40 \text{ mm};\ 16 + d_g) \quad \text{for } f_c \leqslant 60 \text{ MPa} \tag{13}$$

where d_g corresponds to the maximum aggregate size. The value of exponent m corresponds to the slope of the size effect law observed in the double-log scale diagram of Fig. 9. Its value is assumed in the following equal to 3 according to prEN 1992-1-1:2018 [71] for similar problems. This leads to a constant slope of the size effect in double-log scale equal to −1:3, which was observed to be a safe estimate of the results shown in Fig. 9 for the range of typical dimensions related to the bond phenomenon.

5.4. Considerations on casting position and tensile strength

Consistently to the experimental results by other authors [44,47], it has been observed in this testing programme that the casting position had a significant influence on the spalling resistance. As previously discussed, this influence can be attributed to the phenomena of bleeding and plastic settlement. Bleeding reduces mostly the concrete tensile strength (especially in the vertical direction due to the presence of pores under coarse aggregates [63]), while the plastic settlement is associated to the initiation of cracks around the bar. For design purposes, it is suggested to account for them by means of an additional strength reduction factor (η_{is}):

$$p = \frac{\eta_{is} \cdot \eta_{ct} \cdot f_{ct}}{tan\gamma} \cdot 2\sqrt{\frac{c_y}{\phi} + \left(\frac{c_y}{\phi}\right)^2} \cdot \left(\frac{d_{dg}}{1.6\phi}\right)^{1/m} \tag{14}$$

On the basis of the test results presented in this paper, it will be adopted in the following a constant reduction factor $\eta_{is} = 0.6$ when the disturbances are located in the top layer. As it can be noted, the consideration of both η_{is} and η_{ct} reduces the concrete tensile strength to a value of approximately $0.5 f_{ct}$ (as $\eta_{is} \times \eta_{ct} = 0.48 \approx 0.5$). This is consistent with the distribution of spalling forces according to the tests presented in this paper (refer to Appendix A for comparisons for selected specimens). Although some future work would be required to lead to a more comprehensive definition of this parameter, such approach gives consistent agreement to the different cases, as it will later be shown.

5.5. Consideration of multiple disturbances

The experimental programme has also shown the detrimental effect of groups of narrow-spaced disturbances (Fig. 10b). In these cases, the failure surface of one disturbance can intersects those of the surrounding elements, resulting in the development of horizontal cracks amongst them. Therefore, the spalling failure mechanism presented in Fig. 14 is adapted to account for the group effect, as illustrated in Fig. 15.

In this case, it can be noted that the governing solution is close to $\psi \approx 0^{\circ}$ as the interaction between the failure surfaces of the individual bars takes place for sufficient depth of the concrete cover. In the following, Eq. (10) will thus be adopted for consideration of multiple disturbances.

Based on geometrical considerations of Fig. 15, one can compute the spacing leading to a group effect as:

$$c_{s,lim} = 2 \cdot \frac{c_y + \phi/2}{sin\gamma} \cdot cos\gamma = \frac{2c_y + \phi}{tan\gamma} \tag{15}$$

Considering a number of n disturbances at a spacing lower than $c_{s,lim}$, the resistance will result:

$$n \cdot p \cdot \phi = \frac{2 \cdot \eta_{is} \cdot \eta_{ct} \cdot f_{ct}}{tan\gamma} \cdot \left(c_y + \frac{\phi}{2}\right) \cdot \left(\frac{d_{dg}}{1.6\phi}\right)^{1/m} + (n-1) \cdot \eta_{is} \cdot \eta_{ct} \cdot f_{ct} \cdot c_s \cdot \left(\frac{d_{dg}}{1.6\phi}\right)^{1/m} \tag{16}$$

$$p = \frac{\eta_{is} \cdot \eta_{ct} \cdot f_{ct}}{n \cdot \phi} \cdot \left(\frac{2c_y + \phi}{tan\gamma} + (n-1) \cdot c_s\right) \cdot \left(\frac{d_{dg}}{1.6\phi}\right)^{1/m} \tag{17}$$

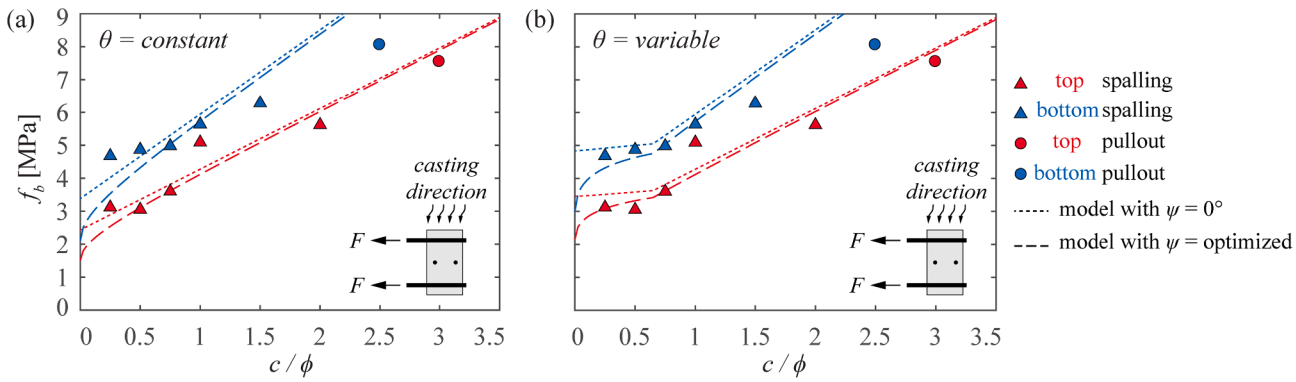

Fig. 19. Main results of the proposed models (dotted lines) and comparison to the pull-out tests performed in current study (triangles and circle markers, series CM11): (a) case with angle of the struts θ constant; and (b) case with θ variable.

5.6. Comparison to test results

The results of the experimental programme are compared in Fig. 16 to the spalling resistance calculated on the basis of the proposed approach for single openings (Eq. (14)) and for multiple openings (Eq. (17)). The results show sound agreement with an average of measured-to-calculated strength of 1.02 and a Coefficient of Variation of 12.3%. If a constant value $\psi = 0°$ were adopted, the overall average becomes 0.98 and the Coefficient of Variation is 12.7%. In general, significant differences between both approaches are only notable for low values of c/ϕ (<1.0), refer to Fig. 16a.

In addition, the results of the test series CM11 (variable cover-to-diameter ratio) are compared to the experimental findings of Williamson and Clark [26] and Morinaga [27]. As shown in Fig. 17, the results of the latter authors follow a similar trend as for the top openings of series CM11 (despite the differences in the diameter of the openings, the dimensions of the specimens, loading rates and that the casting position and direction are not specified). With this respect, the series of Williamson and Clark and of Morinaga were performed on specimens with small dimensions (150–200 mm), leading to comparable conditions as for openings in the upper part of series CM11.

6. Design proposal for pull-out spalling failures

The tests on pull-out specimens showed a complex response in which, just before failure, the out-of-plane displacements were highly variable. According to the performed measurements (refer to Fig. 13), some regions presented out-of-plane displacements larger than those developed at peak strength for tests performed with inflator devices while other regions showed relatively low values. Based on these observations, indicating potential stress redistributions between different regions, the phenomenon of cover spalling due to bond engagement is investigated in this section on the basis of a simple mechanical approach. The approach integrates the information on the response of openings subjected to an internal pressure (as presented in the previous section) by accounting for the observed out-of-plane displacements in pull-out tests.

Following the idealization by Tepfers, it is assumed in the following that the response of a bar being pulled-out is governed by two components, one depending on the pressure developing perpendicular to the cover ($p_\perp$) and another depending on a pressure acting parallel to the cover ($p_{//}$), see Fig. 18a. According to this consideration, equation (1) proposed by Tepfers [1,30,31] can be rewritten as follows:

$$f_b = \lambda \cdot p_\perp \cdot cot\theta_\perp + (1-\lambda)\cdot p_{//} \cdot cot\theta_{//} \tag{18}$$

where coefficient λ denotes the part of bar perimeter associated to each component, that will be set in the following equal to 0.5 for simplicity purposes (future work on this value is however advised to address in a consistent manner the influence of rib orientation and shape).

In absence of specific measurements, it will also be assumed in a simplified manner that $cot\theta_\perp = cot\theta_{//} = cot\theta$, leading to:

$$f_b = \left(\lambda \cdot p_\perp + (1-\lambda)\cdot p_{//}\right)\cdot cot\theta \tag{19}$$

The values of the angle θ (angle between the compressive struts and the bar axis, refer to Fig. 1a) can be obtained from the measurements performed in the experimental programme. To do so, the measured out-of-plane displacements u_y are used to compute the corresponding radial pressure p (which is assumed to account for its two components, i.e. $p = \lambda \cdot p_\perp + (1-\lambda)\cdot p_{//}$). This is performed by using the p-u_y measurements obtained with the inflator devices shown in Fig. 6d-e and considering the difference on the tensile strengths for the two series (refer to values in Table 2). Such value can be eventually associated to a given bond stress (Fig. 12) allowing to determine the $\tau - p$ relationship and consequently the values of θ (by using Eq. (1)). Instances of the calculated angle θ as a function of the slip of the bars δ are shown in Fig. 18b for the complete loading process (case of top bars). From these measurements, it is also possible to select the value of θ at maximum bond strength for each investigated specimen (indicated as bullets in Fig. 18b).

The results referring to the angle θ at maximum bond strength obtained following this procedure are depicted in Fig. 18c-d for top and bottom bars, respectively. As it can be noted, the angle θ is relatively

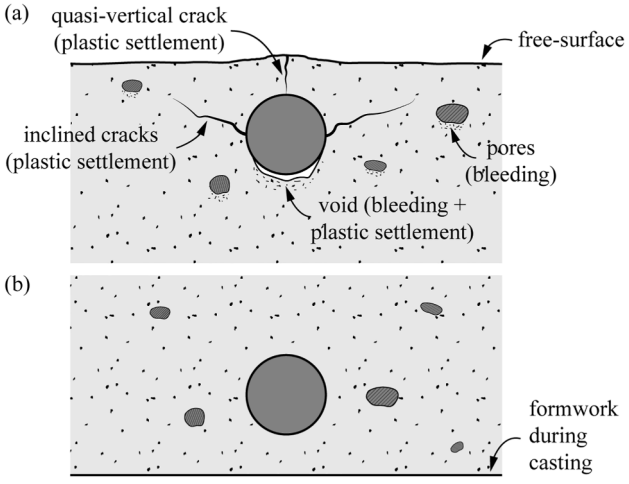

Fig. 20. Influence of casting position effects on the spalling resistance, adapted from [52]: (a) observed cracks types in the region near the top surface (free surface during casting), cracks related to plastic settlement and reduction of the concrete tensile strength due to bleeding; and (b) region near the bottom formwork without cracks due to settlement and without major pores due to bleeding.

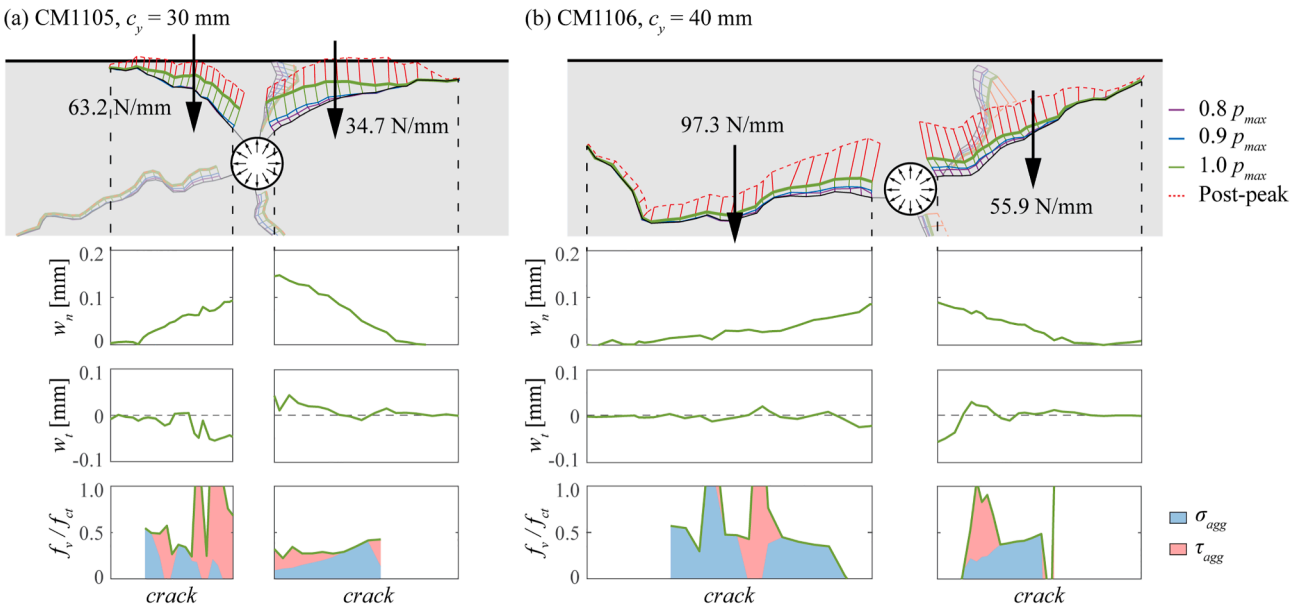

Fig. 21. Resultant of the integration of the shear and normal stresses along the crack at failure according to Cavagnis [72] (w_n: crack opening, w_t: crack sliding, τ_{agg}: shear stresses, σ_{agg}: normal stresses, f_v: vertical force per unit length): (a) specimen CM1105; and (b) specimen CM1106.

constant for the different c_y/ϕ ratios (except for low values of this ratio). Also, a difference between top and bottom bars can be observed, with higher values at failure for bottom bars. As a first estimate of θ, a simplified (constant) value of the angle θ can thus be adopted based on the measurements (Fig. 18c-d) as follows:

$$\begin{aligned} &\theta = 50^\circ \quad \text{(top bars)} \\ &\theta = 55^\circ \quad \text{(bottom bars)} \end{aligned} \tag{20}$$

For a more accurate evaluation of this angle, is it also possible to consider the influence of the ratio c_y/ϕ (Fig. 18c-d):

$$\begin{aligned} &\theta = 40^\circ + 20 \cdot ln\left(1 + \frac{c}{\phi}\right) \leqslant 50^\circ \quad \text{(top bars)} \\ &\theta = 45^\circ + 20 \cdot ln\left(1 + \frac{c}{\phi}\right) \leqslant 55^\circ \quad \text{(bottom bars)} \end{aligned} \tag{21}$$

For evaluation of Eq. (19), the pressure acting perpendicular to the cover $p_\perp$ (related to the radial pressure induced by the wedging action of the ribs) can be estimated on the basis of the pressure p determined with the formulations derived for the case of the application of an internal pressure (refer to Eqs. (14) and (17) for an optimized value of ψ or to Eq. (10) for $\psi = 0^\circ$). With respect to the pressure acting parallel to the concrete cover ($p_{//}$), it is likely to be dependent on the geometry and spacing of the ribs, as well as the state of cracking surrounding the bar. The measurements performed in the experimental programme did not allow for an accurate estimate of this parameter. In the following, for the case investigated experimentally (ribs oriented toward the free surface), a simplified value will be assumed:

$$\begin{aligned} &p_{//,top} = \eta_{is} \cdot p_{//,bot} \\ &p_{//,bottom} = 6.0 \text{ MPa} \end{aligned} \tag{22}$$

where a distinction is made between top and bottom bars, by considering the casting position effects $\eta_{is} = 0.6$.

Based on these considerations, the bond strength at failure can be computed in a simple manner. To do so, Eq. (19) can be used with either constant (Eq. (20)) or variable (Eq. (21)) angles of the struts and the formulations presented in Eqs. (10), (14) and (17) for the radial pressure $p_\perp$ as well as Eq. (22) for the pressure $p_{//}$. This approach is compared in Fig. 19 to the results of current experimental programme. The predictions show consistent agreement with the observed trends of the spalling failures in pull-out conditions. With respect to the formulation with constant values of θ (Fig. 19a), the average of the measured-to-calculated strength results 1.07 with a Coefficient of Variation equal to 14.0% when the angle ψ is optimized. If the angle $\psi = 0^\circ$ is used (Eq. (10)), the average becomes 1.0 and the scatter is lower (Coefficient of Variation of 11.2%).

When the angle θ is considered as variable (see Eq. (21) and Fig. 19b), the formulation of Eq. (19) gives an average of measured-to-calculated strength of 1.01 and Coefficient of variation of 9.9% for an optimized value of ψ. In this case, if $\psi = 0^\circ$ is adopted, the average becomes 0.95 and the Coefficient of Variation is equal to 10.0%.

As it can be noted, the trends are suitably reproduced in all cases. Additional experimental evidence should however be considered for a more comprehensive definition of the angle θ and the component $p_{//}$.

7. Conclusions

This paper presents the results of an investigation on the spalling of concrete cover induced by an internal radial pressure (as can be generated for instance by expansion of rust due to bar corrosion) or by bond in reinforced concrete. The phenomenon is investigated by means of detailed measurements on a series of tests performed with hydraulic inflator devices as well as on pull-out tests of embedded reinforcement. On that basis, the mechanisms triggering failure are identified and reproduced by means of simple mechanical models. The main findings of the paper are summarized below:

1. The spalling response is observed to be relatively different for elements cast in the top and bottom layers due to the phenomena of bleeding and plastic settlement of fresh concrete. Plastic settlement generates cracks radiating from top bars to the surface, which can progress when an internal pressure is applied and eventually become part of a spalling mechanism. Such cracks do not exist on the contrary for bars located near a bottom surface. Bleeding is also associated to a lower tensile strength of the concrete near to the top casting surface, reducing the spalling strength with respect to bars located near to the bottom surface.
2. An analysis of the crack propagation leading to spalling failures shows a more brittle response for elements in the bottom layer when a pressure is applied inside an opening. In this case, failure occurs by a sudden development and propagation of cracks (only quasi-vertical

cracks can develop in a stable manner). On the contrary, for elements in the top layer, the presence of existing cracks due to plastic settlement allows for their controlled propagation until failure. This is associated to a less brittle response.

3. The difference of the response of top and bottom layers in terms of brittleness is also confirmed by means of an analysis of the size effect significance when an internal pressure is applied in the openings. For bottom bars, the observed slopes of the size effect in double-log scale for the cases investigated (in the range corresponding to practical design situations) reach values ranging between −1/5 and −1/3, while the slopes range between −1/10 and −1/5 for top bars. These values are in any case milder than the asymptotic slope corresponding to linear-elastic fracture mechanics (-1/2) and confirm that for practical design purposes, adopting a constant slope equal to −1/3 (as performed by prEN1992-1–1:2018 for similar cases) is a reasonable and safe choice.
4. A model to assess the spalling resistance against a uniform radial pressure is proposed and validated on the basis of the results and observations of the experimental programme. The model is based on a simplified geometry and stress profile of the failure surface, consistently with the analysis performed on actual cracking patterns, and accounts as well for the casting position, size and group effects.
5. Differently to tests subjected to a uniform radial pressure (showing a rather constant out-of-plane displacement along the location where the pressure is applied), pull-out tests show a non-uniform profile of out-of-plane displacements along the bar. Just before failure, some regions display relatively high out-of-plane displacements (associated to regions in softening) while others have low values. This indicates that stress redistributions can potentially occur.
6. The analysis of the out-of-plane displacements of pull-out tests and its comparison to inner-pressure tests allows estimating the angle of the compression struts transferring forces by bond. Based on these measurements together with an estimate of the acting pressures, a simple approach can be proposed to assess the spalling strength of pull-out bars. Such approach shows consistent agreement to experimental evidence and opens a field for future modelling of bond.

Declaration of Competing Interest

The authors declare that they have no known competing financial interests or personal relationships that could have appeared to influence the work reported in this paper.

Acknowledgments

This work was funded by the Swiss Federal Road Office (FEDRO, project No. AGB-2018-001) whose support is greatly appreciated.

Appendix A. Analysis of spalling failures based on detailed measurements of crack development

The use of DIC measurement techniques allowed for accurate observations of the behaviour of the concrete cover and crack propagation at the sides of the members. With respect to tests performed with the hydraulic inflator device, the crack propagation occurred in a stable manner for most of the tests in the top casting position (except for large diameters of openings). However, the propagation was unstable and very brittle for bottom bars (and large diameters openings). In this section, the recorded crack openings and kinematics of the tests performed with the inflator device are used to investigate on the state of stresses developed in the failure region (information later used to develop a design model).

A.1. Tests with stable crack propagation

As previously discussed (refer to Fig. 8), different types of cracks leading to spalling failures were observed: i) cracks inclined towards the free surface, ii) quasi-vertical cracks connecting to the free surface and iii) sub-vertical cracks opposed to the free surface. When the openings are located near to the top surface, cracks of the first two types were already present after casting due to plastic settlement (Fig. 20a) [46,52,68]. Similar patterns were also observed when the disturbances were located near the bottom surfaces, but the cracks did not open until some level of internal pressure was reached (Fig. 8c-d). In fact, in the region near the bottom formwork, the concrete surrounding the opening was not influenced by any previous cracking or reduction of the tensile strength related to bleeding and plastic settlement (Fig. 20b).

On the basis of the crack shape and kinematics, an estimate of the stresses transferred through the cracked surfaces can be obtained. This will be performed following the methodology presented by Cavagnis et al. [72] (refer also to Campana et al. [73]) for shear cracks. This approach [72] accounts for the recorded crack opening (w_n) and sliding (w_t) at every point of a crack. On this basis, the residual tensile strength (depending on w_n) and the contact stresses associated to aggregate interlocking (depending on w_n and w_t) can be determined by means of suitable constitutive laws (Reinhart for the residual tensile strength [74] and expressions consistent with the Two-Phase Model by Walraven [75] for the interlock contribution). By integration of such stresses, the transferred forces across the crack can eventually be determined. Fig. 21a-b shows an instance for two representative cases (specimens CM1105 and CM1106) analysed with this methodology.

As shown in Fig. 21, different responses can be observed depending on the shape and kinematics of the cracks, with contributions to the spalling resistance both of shear (associated to crack sliding) and normal stresses (associated to crack opening). In addition, it can be noted that the cracks are not fully developed at peak load until the free surface, implying the presence of an uncracked concrete region potentially contributing to the spalling resistance (but whose contribution cannot be determined since the measurement of the strains in the uncracked zone was not sufficiently accurate).

With respect to the distribution of the vertical stresses resulting from the normal and tangential stresses acting on the crack surface at failure, it appears that the ratio f_v/f_{ct} varies around a value of approximately 0.5 (despite some level of scatter, see Fig. 21). This indicates that a reduced strength should be considered when assessing the spalling resistance of openings near the top surface. In addition, the horizontal position of the resultant of stresses varies between values of approximately 0.8–1.2 × c_y.

It should be pointed out that the analyses have been performed on the basis of measurements on one side of the member and a potential variation through the thickness of the element is possible. However, Cavagnis et al. [76] noticed that the variations observed within the member's width on the shape of the failure surface transferring shear forces, leads in general to a limited influence on its overall load-carrying capacity.

A.2. Tests with unstable crack propagation

For the tests performed near to the bottom surface, the observed shapes of the cracks were comparable to those performed near to the top surface. However, except for the quasi-vertical crack, all cracks presented almost negligible opening before the peak pressure was attained, when they followed a sudden and unstable propagation (Fig. 8c-d). In this case, the response can be assumed to be governed fundamentally by fracture mechanics considerations (although the asymptotic size effect of linear-elastic fracture mechanics does not apply for the investigated cases as previously discussed) and no conclusions can be drawn on the analysis of the crack surfaces. It is yet interesting to note that, despite the relatively different phenomenon triggering failure, comparable trends to those of tests failing with stable crack propagation were observed. This can for instance be seen in Fig. 9 for the large bar diameter in top position (failing by unstable propagation but with a trend comparable to

the other tests on top position failing with stable crack propagation).

References

[1] Tepfers R. A theory of bond applied to overlapped tensile reinforcement splices for deformed bars. PhD Thesis, Division of Concrete Structures, Chalmers University of Technology, Göteborg, Sweden, 1973. p. 328.
[2] Cairns J, Jones K. The splitting forces generated by bond. Mag Concr Res 1995;47(171):153–65.
[3] International Federation for Structural Concrete. fib Bulletin 10: Bond of reinforcement in concrete. State-of-art report prepared by Task Group Bond Models, Lausanne, Switzerland, 2000, p. 439.
[4] Cady PD, Weyers RE. Deterioration rates of concrete bridge decks. J Transp Eng 1984;110(1):34–44.
[5] Prieto M, Tanner P, Andrade C. Bond response in structural concrete with corroded steel bars. experimental results. In: Modelling of Corroding Concrete Structures, RILEM Bookseries 5. Dordrecht: Springer Netherlands; 2011. p. 231–41.
[6] Balafas I, Burgoyne CJ. Modeling the structural effects of rust in concrete cover. J Eng Mech 2011;137(3):175–85.
[7] Pantazopoulou SJ, Papoulia KD. Modeling cover-cracking due to reinforcement corrosion in RC structures. J Eng Mech 2001;127(4):342–51.
[8] Bhargava K, Ghosh AK, Mori Y, Ramanujam S. Analytical model for time to cover cracking in RC structures due to rebar corrosion. Nucl Eng Des 2006;236(11):1123–39.
[9] Graf O. Versuche über die Widerstandsfähigkeit des Betons an den Abbiegestellen der schief abgebogenen Eisen in Eisenbetonbalken. Deutscher Ausschuss für Eisenbeton, Heft 94, Berlin-München, Germany, 1940. p. 1–55.
[10] Leonhardt F, Walther R, Dieterle H. Versuche zur Ermittlung der Tragfähigkeit von Zugschlaufenstössen. Deutscher Ausschuss für Stahlbeton, Heft 226, Berlin-München, Germany, 1973. p. 1–22.
[11] Stucki D, Thürlimann B. Versuche an Eckverbindungen aus Stahlbeton. Institut für Baustatik und Konstruktion, ETH Zürich, Switzerland, Nr. 8701-1, 1990. p. 1–68.
[12] Franz G, Fein HD. Tests on R/C Culvert and Tunnel Lining, 2nd test series ('Betonversuche mit Baustahlgewebe-Bewehrungen für Rohre und Tunnelverkleidungen, Versuchsreihe 2'). Baustahlgewebe Berichte aus Forschung und Technik, Heft 8, Düsseldorf-Oberkassel, Germany, 1971. p. 52.
[13] Fein HD, Zwissler U. Accomodating Deviation Forces of Curved Reinforcing Bars with Concrete ('Aufnahme von Umlenkkräften aus stetig gekrümmten Bewehrungsstäben durch den Beton'). Die Bautechnik 1974;51(2):58–61.
[14] Neuner J, Stöckl S. Research on Accommodating Deviation Forces of Curved Reinforcing Bars with Concrete Cover and Stirrups ('Versuche zur Aufnahme der Umlenkkräfte von gekrümmten Bewehrungsstäben durch Betondeckung und Bügel'). Deutscher Ausschuss für Stahlbeton, Heft 322, Berlin-München, Germany, 1981. p. 71–106.
[15] Intichar M. Investigation on the Interaction between Bond Stresses and Deviation Stresses (Untersuchung der Interaktion zwischen Verbundspannungen und Umlenkspannungen). Technische Universität Graz, Insitut für Betonbau, Graz, Austria, 2002. p. 95.
[16] Fernández Ruiz M, Plumey S, Muttoni A. Interaction between bond and deviation forces in spalling failures of arch-shaped members without transverse reinforcement. ACI Struct J 2010;107(3):346–54.
[17] Krefeld W, Thurston CW. Contribution of longitudinal steel to shear resistance of reinforced concrete beams. ACI J Proc 1966;63(3):325–44.
[18] Baumann T. Versuche zum Studium der Verdübelungswirkung der Biegezugbewehrung eines Stahlbetonbalken. Deutscher Ausschuss für Stahlbeton, Heft 210, Berlin-München, Germany, 1970. p. 43–83.
[19] Soroushian P, Obaseki K, Rojas M, Najm HS. Behavoir of bars in dowel action against concrete cover. ACI Journal 1987;84(2):170–6.
[20] Vintzēleou EN, Tassios TP. Mathematical models for dowel action under monotonic and cyclic conditions. Mag Concr Res 1986;38(134):13–22.
[21] Dei Poli S, Di Prisco M, Gambarova PG. Cover and stirrup effects on the shear response of dowel bar embedded in concrete. ACI Struct J 1993;90(4):441–50.
[22] Klingsch EWH. Explosive spalling of concrete in fire. Institut für Baustatik und Konstruktion, Bericht Nr. 356, ETH, Zürich, Switzerland, 2014. p. 251.
[23] International Federation for Structural Concrete. fib Bulletin 38: Fire design of concrete structures. State-of-art report, Lausanne, Switzerland, 2007. p. 106.
[24] Bažant Z. Physical model for steel corrosion in concrete sea structures – application. J Struct Division Proc Am Soc Civ Eng 1979;105(6):1155–66.
[25] Bažant Z. Physical model for steel corrosion in concrete sea structures – theory. J Struct Division Proc Am Soc Civ Eng 1979;105(6):1137–53.
[26] Williamson SJ, Clark LA. Pressure required to cause cover cracking of concrete due to reinforcement corrosion. Mag Concr Res 2000;52(6):455–67.
[27] Morinaga S. Prediction of service lives of reinforced concrete buildings based on the rate of corrosion. Special Report No. 23, Institute of Technology, Shimuzu Corporation, 1988.
[28] Allan ML, Cherry BW. Factors controlling the amount of corrosion for cracking in reinforced concrete. Corrosion 1992;48(5):426–30.
[29] Noghabai K. Splitting of concrete covers - a fracture mechanics approach. Fracture Mechanics of Concrete Structures, Proceedings FRAMCOS-2, Aedificatio Publishers, Freiburg, Germany, 1995. p. 1575–84.
[30] Tepfers R. Cracking of concrete cover along anchored deformed reinforcing bars. Mag Concr Res 1979;31(106):3–12.
[31] Tepfers R. Lapped tensile reinforcement splices. ASCE J Struct Divis 1982;108(1):283–301.
[32] Tirassa M, Fernández Ruiz M, Muttoni A. An interlocking approach for the rebar-to-concrete contact in bond. Mag Concr Res 2020:1–15. https://doi.org/10.1680/jmacr.20.00209.
[33] Cairns J. An analysis of the ultimate strength of lapped joints of compression reinforcement. Mag Concr Res 1979;31(106):19–27.
[34] Giuriani E, Plizzari G, Schumm C. Role of stirrups and residual tensile strength of cracked concrete on bond. J Struct Eng 1991;117(1):1–18.
[35] Giuriani E, Plizzari GA. Local bond-slip law after splitting of concrete ('Legami locali dell'aderenza in presenza di fessure di splitting'). Studi e Ricerche, School for the Design of R/C Structures, Milan University of Technology, vol. 7, 1985. p. 57–118.
[36] Giuriani E, Rosati GP. Behaviour of concrete elements under tension after cracking ('Comportamento di elementi tesi di calcestruzzo in fase fessurata'). Studi e Ricerche, School for the Design of R/C Structures, Milan University of Technology, vol. 8, 1986. p. 65–82.
[37] Darwin D, McCabe S, Idun E, Schoenekase S. Development length criteria: bars not confined by transverse reinforcement. ACI Struct J 1992;89(6):709–20.
[38] Gambarova PG, Rosati GP. Bond and splitting in bar pull-out: Behavioural laws and concrete cover role. Mag Concr Res 1997;49(179):99–110.
[39] Gambarova PG, Rosati GP, Zasso B. Steel-to-concrete bond after concrete splitting: test results. Mater Struct 1989;22(1):35–47.
[40] Gambarova PG, Rosati GP, Zasso B. Steel-to-concrete bond after concrete splitting: constitutive laws and interface deterioration. Mater Struct 1989;22(5):347–56.
[41] Gambarova PG, Rosati GP. Bond and splitting in reinforced concrete : Test results on bar pull-out. Mater Struct/Materiaux et Construct 1996;29(5):267–76.
[42] Malvar LJ. Bond of reinforcement under controlled confinement. Technical Report N-1833, Naval Civil Engineering Laboratory, Port Hueneme, California, USA, 1991. p. 40.
[43] Nielsen MP, Hoang LC. Limit analysis and concrete plasticity. third ed. Boca Raton, FL, USA: CRC Press, Taylor ** Francis Group, 2011. p. 788.
[44] Schenkel M. Zum Verbundverhalten von Bewehrung bei kleiner Betondeckung. PhD Thesis, Institut für Baustatik und Konstruktion, ETH, Zürich, Switzerland, 1998. p. 162.
[45] Schenkel M, Vogel T. Versuche zum Verbundverhalten von Bewehrung bei mangelhafter Betondeckung. Institut für Baustatik und Konstruktion, ETH, Zürich, Switzerland, 1997. p. 92.
[46] Castel A, Vidal T, Viriyametanont K, François R. Effect of reinforcing bar orientation and location on bond with self-consolidating concrete. ACI Struct J 2006;103(4):559–67.
[47] Jirsa JO, Breen JE. Influence of Casting position and shear on development and splice length - design reccomendations. Report No. 242-3F, Centre for Transportation Research, The University of Texas at Austin, Austin, TX, USA, 1981. p. 45.
[48] Welch GB, Patten BJF. Bond strength of reinforcement affected by concrete sedimentation. J Ame Concr Inst 1965;62(2):251–64.
[49] Brettmann BB, Darwin D, Donahey RC. Bond of reinforcement to superplasticized concrete. ACI J 1986;83(12):98–107.
[50] Dybel P, Walach D, Ostrowski K. The top-bar effect in specimens with a single casting point at one edge in high-performance self-compacting concrete. J Adv Concr Technol 2018;16(7):282–92.
[51] Cairns J. Influence of casting position on lap and anchorage strength. Heriot Watt University, Edinburgh, UK, 2018. p. 40.
[52] Moccia F, Kubski X, Fernández Ruiz M, Muttoni A. The influence of casting position and disturbance induced by reinforcement on the structural concrete strength. Struct Concr 2020:1–28.
[53] EN 197-1:2011. Cement - Part 1: Composition, specifications and conformity criteria for common cements. Brussels, Belgium: European Committee for Standardization (CEN), 2011. p. 38.
[54] EN 13670:2013. Execution of concrete structures. Brussels, Belgium: European Committee for Standardization (CEN), 2013. p. 66.
[55] EN 206+A1:2016-11. Concrete - Specification, performance, production and conformity. Brussels, Belgium: European Committee for Standardization (CEN), 2016. p. 102.
[56] EN 12350-2:2019. Testing fresh concrete - Part 2: Slump test. Brussels, Belgium: European Committee for Standardization (CEN), 2019. p. 8.
[57] EN 12350-5:2019. Testing fresh concrete - Part 5: Flow table test. Brussels, Belgium: European Committee for Standardization (CEN), 2019. p. 12.
[58] Tasevski D, Fernández Ruiz M, Muttoni A. Assessing the compressive strength of concrete under sustained actions: From refined models to simple design expressions. Struct Concr 2019;20(3):971–85.
[59] International Federation for Structural Concrete. fib Model Code for Concrete Structures 2010. Berlin, Germany: Ernst ** Sohn, 2013. p. 434.
[60] EN ISO 6892-1:2016. Metallic materials - Tensile testing - Part 1: Method of test at room temperature. Brussels, Belgium: European Committee for Standardization (CEN), 2016. p. 79.
[61] GDS Instruments. Copyright," 2020.
[62] Correlated Solutions. VIC-3D Digital Image Correlation. Copyright 1998-2018 Correlated Solutions, Inc.
[63] Giaccio G, Giovambattista A. Bleeding: Evaluation of its effects on concrete behaviour. Mater Struct 1986;19(4):265–71.
[64] Moccia F, Yu Q, Fernández Ruiz M, Muttoni A. Concrete compressive strength: From material characterization to a structural value. Struct Concr 2020:1–21.
[65] Bažant ZP, Sener S. Size effect in pullout tests. ACI Mater J 1988;85(5):347–51.
[66] Fernández Ruiz M, Muttoni A, Sagaseta J. Shear strength of concrete members without transverse reinforcement : A mechanical approach to consistently account for size and strain effects. Eng Struct, Elsevier 2015;99:360–72.

[67] Fernández Ruiz M, Muttoni A. Size effect in shear and punching shear failures of concrete members without transverse reinforcement: Differences between statically determinate members and redundant structures. Struct Concr 2018;19(1):65–75.
[68] Combrinck R, Steyl L, Boshoff WP. Interaction between settlement and shrinkage cracking in plastic concrete. Constr Build Mater 2018;185:1–11.
[69] Brantschen F, Faria DMV, Fernández Ruiz M, Muttoni A. Bond behaviour of straight, hooked, U-shaped and headed bars in cracked concrete. Struct Concr 2016;17(5):799–810.
[70] Goto Y. Cracks formed in concrete around deformed tension bars. ACI Journal 1971;68(4):244–51.
[71] prEN 1992-1-1:2018. Eurocode 2: Design of concrete structures - Part 1-1: General rules, rules for buildings, bridges and civil engineering structures. Brussels, Belgium: European Committee for Standardization (CEN), 2018. p. 293.
[72] Cavagnis F, Fernández Ruiz M, Muttoni A. A mechanical model for failures in shear of members without transverse reinforcement based on development of a critical shear crack. Eng Struct 2018;157:300–15.
[73] Campana S, Fernández Ruiz M, Anastasi A, Muttoni A. Analysis of shear-transfer actions on one-way RC members based on measured cracking pattern and failure kinematics. Mag Concr Res 2013;56(6):386–404.
[74] Reinhardt HW. Fracture mechanics of an elastic softening material like concrete. Heron 1984;29(2):1–42.
[75] Walraven JC. Fundamental analysis of aggregate interlock. J Struct Divis 1981;107(11):2245–70.
[76] Cavagnis F, Fernández Ruiz M, Muttoni A. An analysis of the shear-transfer actions in reinforced concrete members without transverse reinforcement based on refined experimental measurements. Struct Concr 2018;19(1):49–64.